Urban Climate 49 (2023) 101446

Contents lists available at ScienceDirect

Urban Climate

journal homepage: www.elsevier.com/locate/uclim

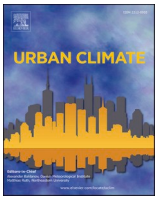

Source apportionment of $PM_{2.5}$ before and after COVID-19 lockdown in an urban-industrial area of the Lisbon metropolitan area, Portugal

Carla A. Gamelas [a,b,*], Nuno Canha [a], Ana Vicente [c], Anabela Silva [d], Sónia Borges [d], Célia Alves [c], Zsofia Kertesz [e], Susana Marta Almeida [a]

[a] Centro de Ciências e Tecnologias Nucleares, Instituto Superior Técnico, Universidade de Lisboa, Estrada Nacional 10, 2695-066 Bobadela, Portugal
[b] Instituto Politécnico de Setúbal, Escola Superior de Tecnologia de Setúbal, Centro de Investigação em Energia e Ambiente, IPS Campus, 2914-508 Setúbal, Portugal
[c] CESAM—Centre for Environmental and Marine Studies, Department of Environment and Planning, University of Aveiro, 3810-193 Aveiro, Portugal
[d] Câmara Municipal do Seixal, Divisão de Desenvolvimento Estratégico, Gabinete Seixal Sustentável e Inovação, 2844-001 Seixal, Portugal
[e] Laboratory for Heritage Science, Institute for Nuclear Research, H-4026 Debrecen, Hungary

ARTICLE INFO

Keywords:
Particulate matter
PIXE
Urban-industrial area
SARS-CoV-2
Pre- and post-confinement periods
Positive Matrix Factorisation

ABSTRACT

The lockdowns held due to the COVID-19 pandemic conducted to changes in air quality. This study aimed to understand the variability of $PM_{2.5}$ levels and composition in an urban-industrial area of the Lisbon Metropolitan Area and to identify the contribution of the different sources. The composition of $PM_{2.5}$ was assessed for 24 elements (by PIXE), secondary inorganic ions and black carbon. The $PM_{2.5}$ mean concentration for the period (December 2019 to November 2020) was 13 $\pm$ 11 $\mu g.m^{-3}$. The most abundant species in $PM_{2.5}$ were BC (19.9%), SO_4^{2-} (15.4%), NO_3^- (11.6%) and NH_4^+ (5.3%). The impact of the restrictions imposed by the COVID-19 pandemic on the PM levels was found by comparison with the previous six years. The concentrations of all the $PM_{2.5}$ components, except Al, Ba, Ca, Si and SO_4^{2-}, were significantly higher in the winter/pre-confinement than in post-confinement period. A total of seven sources were identified by Positive Matrix Factorisation (PMF): soil, secondary sulphate, fuel-oil combustion, sea, vehicle non-exhaust, vehicle exhaust, and industry. Sources were greatly influenced by the restrictions imposed by the COVID-19 pandemic, with vehicle exhaust showing the sharpest decrease. Secondary sulphate predominated in summer/post-confinement. $PM_{2.5}$ levels and composition also varied with the types of air mass trajectories.

1. Introduction

The study of atmospheric particulate matter (PM) is of utmost importance because of the serious health implications it has on humans (Kim et al., 2015; WHO, 2013). It has been demonstrated that the long-term exposure to $PM_{2.5}$ was responsible for 417,000 premature deaths in Europe in 2018 (EEA, 2020). PM produces toxic effects according to their physical and chemical properties

* Corresponding author at: Centro de Ciências e Tecnologias Nucleares, Instituto Superior Técnico, Universidade de Lisboa, Estrada Nacional 10, 2695-066 Bobadela, Portugal.
E-mail addresses: carla.gamelas@ctn.tecnico.ulisboa.pt (C.A. Gamelas), nunocanha@ctn.tecnico.ulisboa.pt (N. Canha), anavicente@ua.pt (A. Vicente), celia.alves@ua.pt (C. Alves), zsofi@atomki.hu (Z. Kertesz), smarta@ctn.tecnico.ulisboa.pt (S.M. Almeida).

https://doi.org/10.1016/j.uclim.2023.101446
Received 25 October 2022; Received in revised form 6 January 2023; Accepted 11 February 2023
Available online 16 February 2023

(Harrison and Yin, 2000). Many $PM_{2.5}$-bound organic constituents and metals have been associated with increased hospital admissions (Zanobetti et al., 2009), and namely Fe, Cr, Cu and Mn may result in pulmonary and heart diseases (Cakmak et al., 2014) and polycyclic aromatic hydrocarbons, Cd, Cr and Ni contribute to high carcinogenic risks (Gao et al., 2016).

The year 2020 begun with the outbreak of a new disease, COVID-19, which was declared a pandemic by the World Health Organisation (WHO) on March 11, following which strict measures as quarantines, restrictions of movements, curfews and lockdown of entire cities were implemented worldwide (He et al., 2020; University of Oxford and Blavatnik School of Governement, 2020). The first confirmed case in Portugal was on March 2, on March 16 schools were closed and the state of emergency was decreed on March 18 (Presidência da República, 2020) until May 4, imposing the general duty of home confinement, mandatory adoption of teleworking and closure of non-essential services.

The restriction measures reduced mobility and minimised anthropogenic activities in an unprecedented way around the world, creating a unique opportunity for assessing the effect of anthropogenic activities on air pollutants (Querol et al., 2021) and on the associated health risks (Aix et al., 2022; Cai et al., 2022). Many studies have reported that air quality has improved significantly during the city lockdowns, due to a drastic reduction of primary pollutants (Collivignarelli et al., 2020; He et al., 2020; Rodríguez-Urrego and Rodríguez-Urrego, 2020; Sharma et al., 2020), while increased secondary pollutant levels were reported (Hong et al., 2021; Wang et al., 2021a; Chang et al., 2020; Zheng et al., 2020; Chang et al., 2022; Ma et al., 2022), underlying the need to understand more deeply the formation mechanisms of secondary $PM_{2.5}$.

There are some studies that report the comparison of $PM_{2.5}$ chemical composition and source contributions in the pre- and post-confinement periods (Hong et al. (2021); Cheng et al. (2022); Cui et al. (2020); Fatima et al. (2022); Li et al. (2021); Zheng et al. (2020); Nguyen et al. (2022); Wang et al. (2021a) and Chang et al. (2020)), but only few are relative to European urban-industrial areas (Massimi et al. (2022); Hicks et al. (2021)) and none to Portugal, to the best of our knowledge.

In Seixal, a highly populated urban-industrial area in the Lisbon Metropolitan Area, comprising heavy industry such as steelworks, and crossed by highways with high density commuting traffic, has suffered from poor air quality in the last decades (Gamelas et al., 2021). Occasional settled dust events, when houses, cars, plants etc. were covered by dust (coarse particles of a granulometric dimension much higher than PM_{10}) have increased the population's concerns regarding the impacts of the air pollution on their health, leading the local Council of Seixal to promote actions, such as the assessment of the chemical composition of the settled dust to determine its sources (Justino et al., 2019) and an air biomonitoring study using lichens in the area (Abecasis et al., 2022). In both studies, the influence of the steel industries was identified due to the content of Fe, Cr and Mn, along with the traffic influence. In fact, although measures have been implemented in many of the steel operations to abate emissions, important amounts of PM are still produced, namely from diffuse emissions (Almeida et al., 2015). Steelworks have been identified as major emission sources of metal (loid)s such as Fe, Mn, Cr, Zn, Pb, As, Cd, Cu, Ni, Se and V (Lage et al., 2016; Taiwo et al., 2014).

In a previous study (Gamelas et al., 2021), where the temporal variability of the concentrations of air pollutants (NO_2, O_3, $PM_{2.5}$, PM_{10} and SO_2) was assessed in Seixal, with an emphasis on the last six years, a significant improvement in air quality regarding PM_{10} and NO_2 was found due to the COVID-19 lockdown, but O_3 and SO_2 levels did not follow that trend, especially in summer.

The present study aimed to identify, for the first time, emission sources and quantify their contributions to $PM_{2.5}$ in Seixal. To

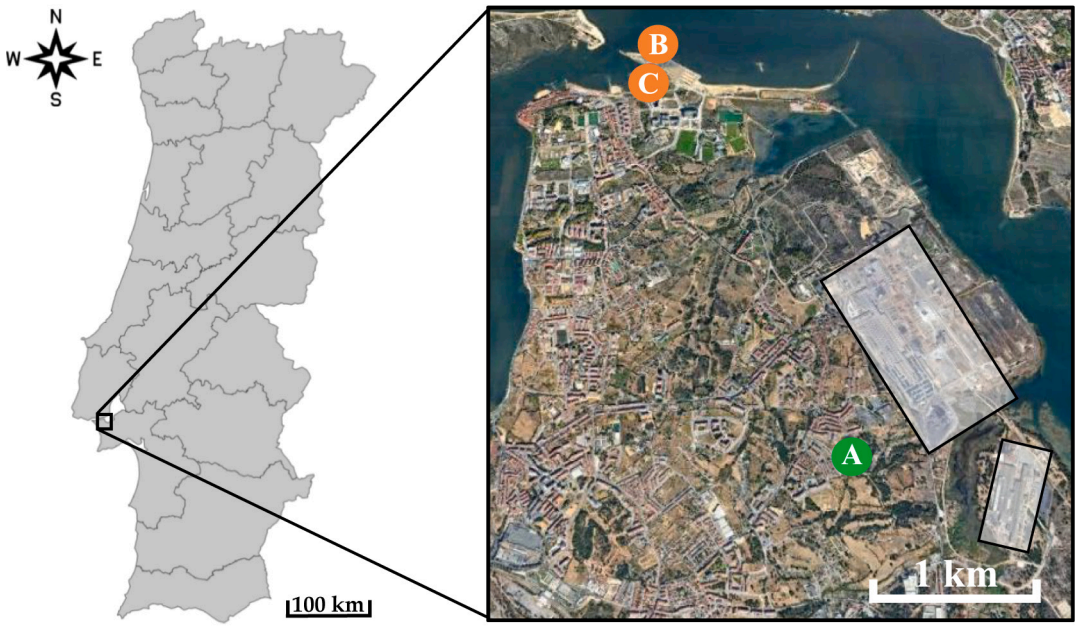

Fig. 1. Location of the sampling site: (left) Framework of the study area (black rectangle); (right) A – sampling site, B – ferry terminal, C – shipyard, and whitish rectangle – industrial area.

achieve this, the concentrations of selected elements, secondary inorganic ions and black carbon in $PM_{2.5}$ were analysed and Positive Matrix Factorisation (PMF), a widely used receptor model (Almeida et al., 2020; Belis et al., 2013; Viana et al., 2008), was applied to identify and apportion the emission sources to which the residents of Seixal were exposed to, before and after the COVID-19 confinement, a knowledge that is critical to design effective $PM_{2.5}$ mitigation strategies in the near future.

2. Materials and methods

2.1. Study site

PM was sampled at Aldeia de Paio Pires (38.617885°, −9.080055°), located in the municipality of Seixal (Portugal), a suburban and industrial area in the Metropolitan Area of Lisbon (Fig. 1). Seixal is one of the most densely populated municipalities in Portugal, with 167,294 inhabitants in 95.5 km^2 (PORDATA, 2022). The sampling site is at 2–3 km from high density traffic highways (A2-IP7 and A33), and is surrounded by small and medium-sized industries, as well as an industrial park (at 1 km) (Abecasis et al., 2022): a steelworks that manufactures galvanised sheet metal; an Electric Arc Furnace steelworks; a lime factory involving the calcination of limestone in a coke kiln; and a metal waste management and treatment factory. Furthermore, the sampling site is at 3.5 km distance from a shipyard and the ferry terminal that connects the two river banks for commuting (Fig. 1).

2.2. Particulate matter sampling

Sampling was carried out in 24 h periods, starting at 10:00 GMT (except for Sundays, when sampling begun at 0:00 GMT), in 128 sampling days, from December 2019 to November 2020, except in the months of April and May, where no sampling was carried out because of the COVID-19 lockdown. Three sampling campaigns are distinguished: winter (from December 18, 2019 to March 18, 2020), summer (from June 15 to August 9, 2020) and autumn (from September 21 to November 12, 2020). Two periods are distinguished: the pre-confinement period, prior to the state of emergency decreed in March 18, 2020 (Presidência da República, 2020) and the post-confinement period, after May 2, 2020 when the state of emergency ended (Assembleia da República, 2021) and when less restrictive regulations were applied.

PM sampling was conducted using two medium volume samplers (MVS6, Leckel, Sven Leckel, Germany) that worked in parallel, equipped with a new sampling head developed by the Institute of Nuclear and Radiological Sciences and Technology, Energy and Safety, N.C.S.R. Demokritos, for the simultaneous collection of $PM_{2.5}$ and $PM_{2.5–10}$, at a constant flow rate of 2.3 m^3/h. The quality assurance and control of the new heads was described by Faria et al. (2020). One sampler collected $PM_{2.5}$ on PTFE filters (SKC) of 47 mm diameter and pore of 2.0 μm and $PM_{2.5–10}$ in PTFE filters (Pall) with 25 mm diameter and pore of 0.5 μm. The other sampler collected $PM_{2.5}$ on quartz filters (Pall) of 47 mm diameter, and $PM_{2.5–10}$ on quartz filters of 25 mm diameter.

$PM_{2.5}$ and PM_{10} concentrations corresponding to the sampling days and also PM_{10} concentrations for the years 2014–2019, were obtained for comparison from the Paio Pires monitoring station (38.621028°, −9.082056°) of the National Air Quality Monitoring Network, operated by the Portuguese Environmental Agency (APA), through the national information system QualAr (APA, 2022).

2.3. Gravimetric analysis

The filter loads were measured by gravimetry in a clean room (class 10,000). The weight of PTFE filters, before and after sampling, was obtained using a 0.1 μg sensitivity balance (Mettler Toledo UMT5), as the average of three measurements, when observed variations were <0.3 μg. The uncertainties in mass loading assessment were lower than 0.8% for all samples in 47 mm PTFE filters and 0.3% for 25 mm PTFE filters.

The PM concentrations determined gravimetrically show a good correlation with the concentrations obtained from the QualAr database (APA, 2022), for the Paio Pires air quality monitoring station, with $r^2 = 0.74$ and 0.89 and gradient of the least squared fitted lines 1.03 and 1.08, for $PM_{2.5}$ for PM_{10}, respectively (Fig. S3). The mean $PM_{2.5}$ and PM_{10} concentrations of the Paio Pires monitoring station in the sampling period (10 ± 8 and 22 ± 12 $\mu g.m^{-3}$, respectively) were not significantly different from the PM concentrations determined by the gravimetric reference method in this work (p-value >0.050).

2.4. Chemical analysis

2.4.1. Elements

The samples collected in PTFE filters were used for elemental analysis by Particle Induced X-Ray Emission (PIXE). PIXE analysis was conducted in the Tandetron Laboratory of ATOMKI, Debrecen, Hungary using the new external millibeam PIXE setup during two measurement campaigns, November 2020 and June 2021. The irradiation of the samples was performed at the left 45° beamline of the ATOMKI 2MV Tandetron accelerator (Rajta et al., 2018) with a proton beam of 2.5 MeV energy and of 15–20 nA current. The accumulated charge on each sample was 10 mC. During the irradiation the samples were scanned in front of the beam in order to reduce the risk of degradation and to increase the analysed area. In November 2020 the characteristic X-rays were recorded by an ultra-thin window (UTW) Rayspec SDD detector with 30 mm^2 area and a Canberra type Si(Li) detector with 50 mm^2 active area. The UTW SDD was equipped with a pair of 4 cm long permanent magnet which protects the detector from the scattered protons, while a 125 mm thick Kapton absorber was used in front of the SiLi detector. In June 2021, a detector cluster containing 4 SDD X-ray detectors were applied. One of the detectors was the above mentioned ultra-thin windowed SDD equipped with the pair of magnets. Three 65 mm^2

SDD detector with Be window (12.5 μm thick) and a kapton absorber of 125 mm thickness made the cluster complete. In order to improve the analytical performance, spectra recorded by the 3 identical SDD detectors was summarized. This case excellent detection limits were achieved. The irradiation dose was measured by integrating the current on a Faraday cup placed behind the samples. The PIXE measurements were performed in He atmosphere (2 l/min flow rate), which enables the detection of X-rays down to 0.35 keV on the UTW SDD. Detailed description of the setup can be found in Aljboor et al. (2023). PIXE spectra was evaluated with the GUPIXWIN program code (Campbell et al., 2010) handling the samples as 'thin' specimen. The elemental composition of $PM_{2.5}$ in sampled filters was assessed for a total of 24 elements after blank corrections (Al, As, Ba, Br, Ca, Cl, Cr, Cu, Fe, K, Mg, Mn, Na, Ni, Pb, Rb, S, Se, Si, Sr, Ti, V, Zn, and Zr), although As, Rb, Sr and Zr are not presented since these elements were quantified in <40% of the samples. PIXE spectra by the UTW-SDD provided the concentrations of low-Z elements (Na – Fe) while concentrations of elements with Z > 19 (K—Pb) were calculated from spectra recorded by the SDD cluster or the Si(Li) detectors. Concentrations of elements common in the two spectral ranges (e.g. K, Ca, Ti, Fe) were used to check the goodness of the measurement parameters and evaluation. The accuracy of the PIXE analytical method was evaluated with NIST SRM2783 filter standard and the results for all applied X-ray detectors are presented in Table S1. The obtained concentrations for all detected elements were within uncertainty to the certified or reference values. The fit errors (%) were: Mg, Al, Si, Ca, Fe (1), K (2), S and Ti (4), P (7), Zn (9), Cl (10), Mn (16), Na (18), Cu (28), Ni (39), Cr (57). Analytical uncertainty ranged from 5 to 30%, depending on the elements fit error and concentration (Table S1). The detection limits for the measured elements are provided in Table S2. The Quality Control of the PIXE measurements were done according to best practices: at least one sample per sample holder was re-measured, while PIXE analysis on reference materials was performed on each day of the measurement campaign. In addition, in November 2020 all samples were measured in He flow of 2 l/min and in normal atmospheric conditions. The obtained concentrations were the same within 5% uncertainty.

2.4.2. Water-soluble inorganic ions

Quartz fiber filters were used for the determination of water-soluble inorganic ions (SO_4^{2-}, NO_3^- and NH_4^+). The analyses were performed at the Department of Environment and Planning of the University of Aveiro, according to the methodology detailed in Vicente et al. (2018). The uncertainty of the determinations (mean uncertainty ± s.d.) was: SO_4^{2-} 100 ± 23, NO_3^- 72 ± 47 and NH_4^+ 84 ± 26 ng.m^{-3}. Half of the filter was extracted with ultrapure water (< 18.2 MΩ cm) by ultrasonication (Sonorex RK156, Bandelin) for 30 min (3 extractions of 10 min each, with a 5 min stop between them). Filtration through a pre-washed PVDF (Polyvinylidene Fluoride) filter of 13 mm diameter and 0.2 μm pore (WhatmanTM) was then performed and the filtered aqueous extracts were analysed by ion chromatography. For the analysis of anions, an ICS-3000 SP (DIONEX, USA) pump and an injection system Gilson model 401/231, and a column oven CTO-6A (Shimadzu) with a conductivity cell connected to the Shimadzu CDD-6A conductimeter were employed. A Dionex AG14 (4 × 250 mm) pre-column was placed between the injector and the Dionex AS14 (4 × 250 mm) analytical column. A Dionex AMMS II suppressor was used. The system was operated with a 50 μL loop, a reading range of 64 μS/cm and a gain of 0.1. H_2SO_4 (50 mM) and $Na_2CO_3 + NaHCO_3$ were used as regenerating solution and eluent, respectively, both with a flowrate of 2 mL.min^{-1}. For the analysis of cations, a Dionex DX-100 system was used, with a Gilson 234 injector, a Dionex CS12 column (4 × 250 mm), a Dionex CG12A (4 × 50 mm) pre-column and a suppressor (Dionex CMMS III). The system was operated with a 100 μL loop and a reading range of 100 μS/cm. A regenerating solution of tetrabutylammonium hydroxide (TBA) (100 mM) and an eluent solution of H_2SO_4 (25 mM), diluted in ultrapure water, were used at a flow rate of 1 mL.min^{-1}. Blank PTFE and quartz filters were treated the same way as regular samples and concentrations were corrected by subtracting the filter blank contents.

2.4.3. Black carbon

A Multi-wavelength Absorption Black Carbon Instrument (MABI) developed by ANSTO, was used to measure BC in $PM_{2.5}$ sampled in the 47 mm PTFE filters. The light transmission was measured through unexposed filters (I_0) and sampled filters (I) and the BC mass concentrations (in ng.m^{-3}) were determined by eq. 1 (Manohar et al., 2021):

$$BC(\lambda_{639}) = \frac{10^5.A}{\varepsilon(\lambda_{639}).V} ln\left(\frac{I_0}{I}\right) \quad (1)$$

where $\varepsilon(\lambda_{639})$ is the mass absorption coefficient at $\lambda = 639$ nm, with a value of 6.036 m^2.g^{-1}, A is the sampled filter area (cm^2), and V is the sampled volume of air (m^3). BC determined at $\lambda = 639$ nm ($BC(\lambda_{639})$) corresponds to the total BC, including fossil fuels and biomass burning.

The detection limit (DL) at $\lambda = 639$ nm was determined from the reported minimum detectable limits (Manohar et al., 2021), expressed in ng.cm^{-2}, by multiplying by the filter area A and dividing by the volume V of air through the filter (to convert to ng.m^{-3}). The fractional error estimates were also taken from Manohar et al. (2021), in terms of tiers below, around and above the DL. The uncertainty of the BC determinations (mean uncertainty ± s.d.) was 400 ± 230 ng.m^{-3}.

2.5. Positive Matrix Factorisation

Positive Matrix Factorisation, a widely used receptor model (Paatero, 1999; Paatero et al., 2014), version 5.0 (US-EPA, 2014), was used to identify the main emission sources and estimate their contributions to the $PM_{2.5}$ mass. PMF is based on the mass conservation principle:

$$x_{ij} = \sum_{k=1}^{p} g_{ik} f_{kj} + e_{ij} \; i = 1, 2, \ldots m; j = 1, 2, \ldots n \tag{2}$$

where x_{ij} is the concentration of the species j in the i^{th} sample, g_{ik} is the contribution of the k^{th} source in the i^{th} sample, f_{kj} is the concentration of the species j in the chemical profile of source k, and e_{ij} is the uncertainty of each individual measurement result. Factor contributions and profiles are derived in the EPA PMF 5.0 model by minimizing an objective function Q, without detailed prior knowledge on sources inventories (Paatero, 1999):

$$Q = \sum_{i=1}^{n} \sum_{j=1}^{m} \left[\frac{x_{ij} - \sum_{k=1}^{p} g_{ik} f_{kj}}{u_{ij}} \right]^2 \tag{3}$$

Data matrix was composed by 128 samples and 24 PM species. For a variable to be included, a threshold of at least 70% of points higher than the detection limit (DL) was set. The model was supplied with the number of factors, the concentrations and uncertainties of the components of $PM_{2.5}$. The elements Pb and V were considered "weak" variables in the model; Ba, Cr, Ni, S and Se were considered "bad" variables and were excluded from the analysis (since they did not reach the threshold of at least 70% of points higher than the DL and S would be colinear with SO_4^{2-}). $PM_{2.5}$ mass was used as "total variable". Values below the DL were replaced by 1/2 DL and their uncertainties were set at 5/6 DL. Missing data were replaced by the median of the measured values and the uncertainties were set at four times the median value (US-EPA, 2014). The uncertainties of concentrations were evaluated as described in US-EPA (2014), using eq. 4:

$$Uncertainty = \sqrt{(Error\ fraction.Concentration)^2 + (0.5\ DL)^2} \tag{4}$$

In addition to the analytical uncertainty, extra uncertainty was added in order to account for the sampling uncertainty, using the methodology described in Amato et al. (2009).

The model was repeatedly run (100 times for each solution), with different number of factors/sources ($n = 5$ to 8), and the variation of the Q-values, the scaled residuals, the regression diagnostics (r^2 and slope), and the physical meaningfulness of the sources were assessed. Finally, the $n = 7$ solution was adopted, leading to a solution with 95–100% of the scaled residuals located between the range [−3,3] for all the elements. A percentage difference of 2.4% between Q_{true} and Q_{robust} was found, in the range of values found in intercomparison studies (Almeida et al., 2020).

The Base Model Displacement Error (DISP) method was then used to explore the rotational ambiguity in the PMF final solution (US-

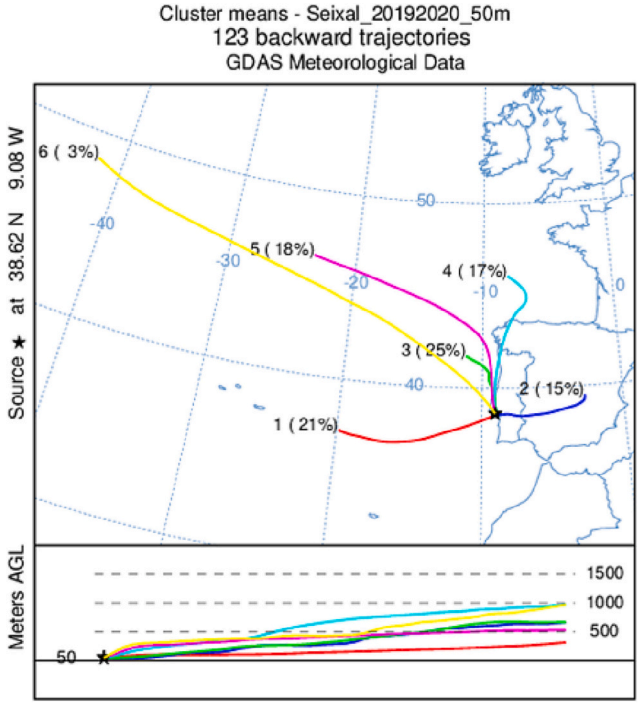

Fig. 2. Average backward trajectories of the clusters calculated with the HYSPLIT model (and percentages of sampling days represented by each cluster).

EPA, 2014). It evaluates the largest range of source profile values without a significant rise in the Q value. The factor profile values are adjusted to the maximum allowable level, with the constraint that the difference between the Q values associated with the original and the modified solutions (dQ) is not greater than a value predefined by the model (dQmax). There was no variation in the Q value in DISP and no factor swaps occurred for all the dQ_{max} values considered, indicating that there was no significant rotational ambiguity. Additionally, the Bootstrap (BS) method was used to assess the uncertainty that originates from random errors in the dataset and partially from rotational ambiguity. BS estimates the random errors on the matrix by altering the original dataset. During BS some rows of the original dataset are deleted while others are repeated. The model then provides a solution for each of the new datasets and the results are compared with the original solution. Base runs were reproduced at least in 86–100% of the factors, considering the correlation value of 0.6, showing that the number of factors (n = 7) is appropriate and the solution is satisfactorily robust (US-EPA, 2014).

2.6. Air mass trajectories

Back-trajectories were simulated using the NOAA/ARL Hybrid Single Particle Lagrangian Integrated Trajectory (HYSPLIT) model version 5.1.0 (Stein et al., 2015) and meteorological data from the Global Data Analysis System (GDAS1). Four days backward trajectories ending at the sampling point, at the start of each sampling day, were calculated using the vertical velocity option and using different starting heights (50, 500 and 1000 m). Back trajectories were clustered using the HYSPLIT module and a cluster number was retained which corresponds to the large variation in Total Spatial Variance percentage (Stunder, 1996).

Air masses were grouped into six clusters of the following classes (Fig. 2 and Fig. S4): M – maritime (clusters 1 and 6); MT - maritime transformed (clusters 3, 4 and 5); C – continental (cluster 2). Four samples could not be clustered.

2.7. Meteorological data

Meteorological data were obtained from the Barreiro-Lavradio weather station (38.674444°, −9.0475°) of Instituto Português do Mar e da Atmosfera - IPMA. During the sampling period, the mean temperature was 17.9 ± 4.8 °C (from 8.5 to 30.0 °C) and the mean relative humidity was 78.2 ± 10.9% (from 42.0 to 99.0%), with a total of 31 rainy days (Fig. S1, Supplementary Information).

Fig. S2 shows the wind roses for each sampling campaign. In winter, there was a predominance of winds from North (N), Northeast (NE) and Southwest (SW), and in summer and autumn, from North (N), Northwest (NW) and Southwest (SW). The predominant winds from N and NE make the sampling site downwind of the industrial park where the steelworks are located, but upwind from the A2 highway which is in the SW direction (Fig. 1).

2.8. Statistical analysis

Statistical calculations were carried out using STATISTICA software version 13. The non-parametric Mann–Whitney *U* test was employed to assess significant differences between two independent groups, at a significance level of 0.050.

3. Results and discussion

3.1. PM mass concentration and chemical composition

3.1.1. PM levels and exceedances

The concentrations of PM and measured constituents of $PM_{2.5}$ are summarized in Table S3 and Fig. S5 (in the Supplementary Information), discriminated by sampling campaign. The mean $PM_{2.5}$ concentration for the whole sampling period was 13 ± 11 $\mu g.m^{-3}$, below the $PM_{2.5}$ annual limit of 20 $\mu g.m^{-3}$ of Directive 2008/50/EC, of 21 May 2008, but higher than the WHO annual guideline value of 5 $\mu g.m^{-3}$ (WHO, 2021). In fact, the WHO daily guideline for $PM_{2.5}$ of 15 $\mu g.m^{-3}$, not to be exceeded >3–4 days per year, has been exceeded 33 times in the 128 sampling days. The PM_{10} mean concentration (24 ± 13 $\mu g.m^{-3}$) was below the EU annual limit of 40 $\mu g.m^{-3}$ and the PM_{10} daily limit value of 50 $\mu g.m^{-3}$, which must not be exceeded >35 times a year, was exceeded 4 times in the 128 sampling days. Nevertheless, the WHO annual guideline value of 15 $\mu g.m^{-3}$ was exceeded (WHO, 2021).

The $PM_{2.5}/PM_{10}$ ratio was 0.49 ± 0.15 (ranging 0.21 from to 0.85) in the whole sampling period (with no significant difference between campaigns), meaning that usually there was an almost equal contribution from both the fine and coarse PM fractions. These values are comparable with the average $PM_{2.5}/PM_{10}$ ratio observed in 20 European areas (0.60) (Eeftens et al., 2012), and with other studies, namely in the vicinities of steelworks, by Mohiuddin et al. (2014) (0.35–0.54) and Almeida et al. (2015) (0.37–0.63).

In the 33 sampling days when the daily WHO guideline for $PM_{2.5}$ (15 $\mu g.m^{-3}$) was exceeded, the $PM_{2.5}/PM_{10}$ ratio was 0.64, significantly higher than in non-exceedance days (*p*-value = 0.000), suggesting an increase in anthropogenic emissions in these days, since anthropogenic sources are known to contribute mainly to $PM_{2.5}$ and natural sources to $PM_{2.5–10}$ (Almeida et al., 2012; Fatima et al., 2022).

The sum of the percentage concentrations of the analysed species (Table S3) represented, on average, 71.8% of $PM_{2.5}$. The remaining fraction can be attributed to OC and carbonate (which were not measured), oxides of soil elements and water retained in the samples at the weighing conditions. The most abundant species in $PM_{2.5}$ were BC (19.9%), SO_4^{2-} (15.4%), NO_3^- (11.6%) (with mean concentrations higher than 1 $\mu g.m^{-3}$) and NH_4^+ (5.3%), which are mainly associated with anthropogenic sources and secondary production mechanisms (in the case of SO_4^{2-}, NO_3^- and NH_4^+) (Calvo et al., 2013). Other major species (above 100 $ng.m^{-3}$) were Na, Cl, K, Ca, Si and Fe. These results were of the same order of magnitude of aerosol data in other urban areas in the Lisbon Metropolitan area

(Almeida-Silva et al., 2020) (Table S3). When these figures are compared to Southern Europe urban sites, where BC (EC) only contributes around 8% to $PM_{2.5}$ mass (Putaud et al., 2010), it can be concluded that the emission of BC in the study area, probably from the highway traffic and industry, is higher. In fact, the mean BC concentration (2510 ± 2010 ng.m^{-3}) was higher than the mean values found in urban background sites of Barcelona (1000 ng.m^{-3}) and Milan (1784 ng.m^{-3}) (Amato et al., 2016), and also higher than the value reported by Healy et al. (2017) for a site near a highway in Canada (1740 ng.m^{-3}), being nevertheless lower than the value in a traffic site in Porto (5006 ng.m^{-3}) (Amato et al., 2016).

Among heavy metals, the most abundant were Fe and Zn, contributing to 1.5% of $PM_{2.5}$. The levels found of Fe, Cr, Mn and Zn (considered tracers of the steel industry (Calvo et al., 2013)) were in the range of values observed in the vicinity of a major steelworks in the UK (Taiwo et al., 2014), but were lower than the mean values observed in sites under the influence of steel manufacture in Spain (Querol et al., 2007) (Table S3).

3.1.2. *Impact of COVID-19 containment measures and seasonality on PM levels and composition*

In the sampling period prior to the first state of emergency (winter/pre-confinement campaign), the $PM_{2.5}$ and PM_{10} mean concentrations (17 ± 14 μg.m^{-3} and 30 ± 16 μg.m^{-3}, respectively) were significantly higher than in the post-confinement period (9.4 ± 6.1 μg.m^{-3} and 19 ± 10 μg.m^{-3}, *p*-value = 0.000), and no significant difference was found between the two post-confinement campaigns (p-value >0.050). Thus, there was a reduction of 46.1% and 35.9% in $PM_{2.5}$ and PM_{10}, respectively, from the pre-pandemic to the pandemic period, a pronounced drop that was certainly due to the confinement measures imposed to halt the COVID-19 pandemic, which led to a reduction in anthropogenic emissions (Chauhan and Singh, 2020). This impact was higher compared to the national level, where there was an average reduction of 18% for PM_{10}, considering 20 monitoring stations dispersed in mainland Portugal (Gama et al., 2021), but it was comparable to the European level, where the largest average reductions in PM_{10}, of about 40% in traffic stations and 30% in urban and suburban stations, were registered in Spain (EEA, 2020). A large span in $PM_{2.5}$ reductions was observed worldwide, as for example, from metropolitan areas in Germany (5%) (Balamurugan et al., 2022), Grenoble (22%) (Aix et al., 2022), Lanzhou (Chang et al., 2022) and North China Plain (Li et al., 2021) (~20%), to Shanghai (Chen et al., 2020a) and Chongqing (Chen et al., 2020b) (30–50%).

Besides the influence of the pandemic, the reduction of $PM_{2.5}$ and PM_{10} may be due in part to the seasonal variability, since PM typically shows higher levels during the cold season, due to the lower mixing layer heights (Granados-Muñoz et al., 2012) and stagnant episodes associated with thermal inversion (Lyamani et al., 2012) that inhibit the dispersion of pollutants in winter. For this reason, a comparison with the previous years should be performed. In fact, the mean PM_{10} concentrations registered in Paio Pires monitoring station in the previous six years (2014-2019) had a significantly higher value of 27 ± 15 μg.m^{-3} (Gamelas et al., 2021) when compared with the PM_{10} mean concentrations found for the 128 sampling days in the present study (24 ± 14 μg.m^{-3}, *p*-value = 0.042), thus confirming the impact of the confinement measures on PM levels.

The change in the emission patterns of air pollutants caused by the pandemic was felt not only in the PM mass concentrations, but also in its chemical composition, as depicted by Fig. 3, which shows that concentrations of all $PM_{2.5}$ components, except for Al, Ba, Ca, Si and SO_4^{2-}, were significantly higher in the winter/pre-confinement than in the post-confinement period (*p*-value <0.050). These results are in line with other works that have shown significant reductions in $PM_{2.5}$ primary components concentrations (e.g. K, Fe, Zn, Ba, Mn, Pb, Cu, As, Ni, Se and Cr, in Cheng et al. (2022); Cr, Fe, Na^+, Cl^-, Pb, Ca, Cr, Cu, Fe, Zn and EC, in Li et al. (2021); Zn, Pb, Mn, As, Cu, Ni, V, Cr, Cd and Co, in Wang et al. (2021b); Cd, Se, As, Sr, Ba, Cu, Mn, Pb, K, Zn, Ca, Al, and Mg, in Nguyen et al. (2022)), attributed as an effect of the measures imposed by the COVID-19 lockdown. Soil elements Al and Si, did not vary significantly, since being of natural origin, were less affected by the reduction of anthropogenic activities.

BC concentrations were significantly higher in the winter/pre-confinement (3450 ± 2520 ng.m^{-3}) than in the post-confinement period (1860 ± 1200 ng.m^{-3}, p-value = 0.000) and no significant difference was found between summer and autumn (post-confinement) campaigns (p-value >0.050). The atmospheric pollutant levels showed different decreasing trends in different sites, in

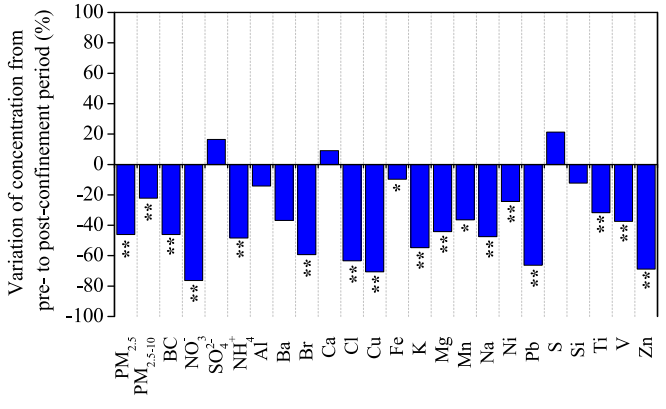

Fig. 3. Variation of concentration of aerosol components from the pre- to post-confinement period. Significantly different concentrations between the two periods are identified with * (p-value <0.050) and ** (p-value <0.010).

line with different intensity of the COVID-19 mitigation measures put in practice, among other factors, such as meteorology. Nevertheless, reductions in BC concentrations have been consistently registered in lockdown periods relative to pre-pandemic conditions, around the globe, namely in Massachusetts/USA (22–46%) (Hudda et al., 2020), Chongqing/China (39%) (Chen et al., 2020b) and Milan/Italy (Collivignarelli et al., 2020), where the highest decrease (by 71%) was noticed.

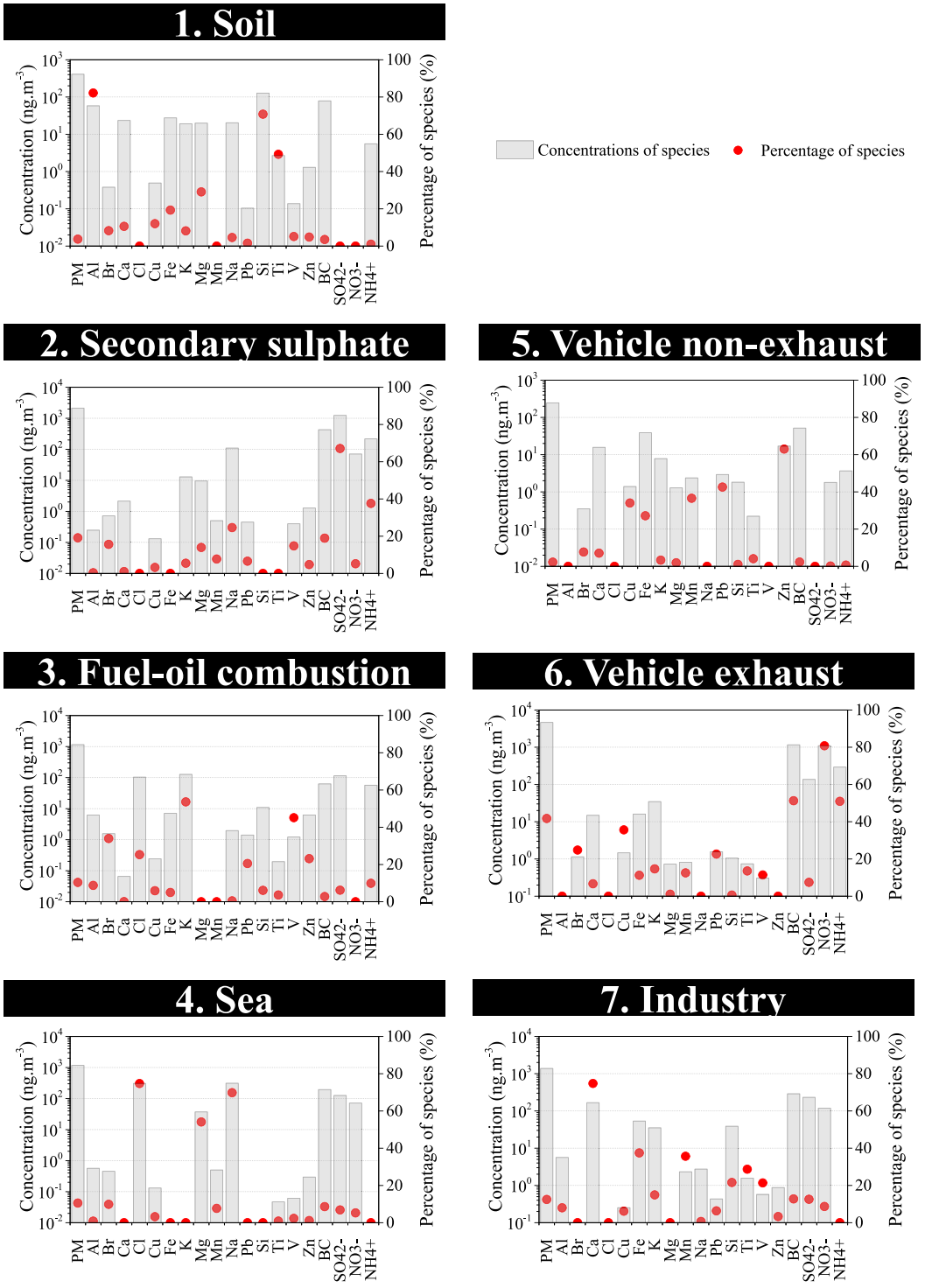

Fig. 4. Source profiles identified by PMF, with concentrations of the species expressed in ng.m^{-3} (bars) and their percentages (red dots) for each source. (For interpretation of the references to colour in this figure legend, the reader is referred to the web version of this article.)

The same trend was observed for NO_3^-, for which the most pronounced reduction (76.4%) was observed, from the winter/pre-confinement (2690 ± 3030 ng.m^{-3}) to the post-confinement period (635 ± 575 ng.m^{-3}, *p*-value = 0.000), with no significant difference between the two post-confinement campaigns (p-value >0.050). This is in line with the concentrations of its gaseous precursor NO_2 in the studied area, which registered significant reductions in the pandemic period of 2020 relative to the previous six-year averages (44.0% in April, 17.4% in May, 29.0% in June and 31.6% in August) (Gamelas et al., 2021). Less pronounced reductions in NO_3^- concentrations were generally observed worldwide (namely 17.6%, in Lanzhou (Chang et al., 2022) and 6.7%, in Linfen (Liu et al., 2022)), but there were also cases in which an increase was observed, as the result of enhanced atmospheric oxidation capacity (Ma et al., 2022).

SO_4^{2-} is an exception in the variations presented by Fig. 3, with summer/post-confinement concentration (3000 ± 1570 ng.m^{-3}) being significantly higher (p-value = 0.000) than in the winter/pre-confinement (1760 ± 1150 ng.m^{-3}) and autumn/post-confinement (1130 ± 770 ng.m^{-3}) campaigns (although there was no significant difference between pre- and post-confinement periods, *p*-value >0.050). The increase in SO_4^{2-} concentration in summer is in good agreement with the increase in the concentrations of its precursor SO_2 found in June (39.6%), July (40.6%), August (30.0%) and September (33.0%) (Gamelas et al., 2021), highlighting the impact of the local industries of the study area, which maintained their typical work flow in these months. The increase in SO_4^{2-} concentration in summer also confirms that SO_4^{2-} tends to increase during the hot season, due to enhanced photochemical activity that promotes the formation of secondary sulphates $(NH_4)_2SO_4$ (Almeida et al., 2006b). In fact, in summer, SO_4^{2-} and NH_4^+ presented a strong correlation (r^2 = 0.80, Fig. S6 - left).

In winter, NH_4^+ associates with NO_3^- instead, as evidenced by the very strong correlation in Fig. S6 (right), due to the shifting of the $NH_4NO_{3(s)} \leftrightarrow HNO_{3(g)} + NH_{3(g)}$ equilibrium to the aerosol phase, under the lower temperatures and higher relative humidity registered in this season (Almeida et al., 2006b), and this also contributes to the higher concentrations of NO_3^- in $PM_{2.5}$ observed in the winter/pre-confinement campaign.

The mass ratio NO_3^-/SO_4^{2-} has been used as an indicator of the relative importance of mobile versus stationary sources of nitrogen and sulphur in the atmosphere (Arimoto et al., 1996). The ratio NO_3^-/SO_4^{2-} took the value of 1.5 in winter/pre-confinement, 0.18 in summer/post-confinement and 0.64 in autumn/post-confinement campaigns, with a significant difference between pre- and post-confinement (p-value = 0.000). This suggests that in winter/pre-confinement traffic emissions prevailed, while in the post-confinement (especially in summer) stationary sources were predominant instead, due to the decrease in commuting mobility and sustained industrial activity in the area, as found in other works (Chang et al., 2022).

3.2. Source apportionment

To identify emission sources and assess their contribution to the sampled $PM_{2.5}$ concentrations, a source apportionment study was conducted using the PMF model. The samples of March 18 and July 20, when Sahara dust events occurred resulting in peak concentrations of Si, Al, Ca and Fe in $PM_{2.5}$ (Fig. S7), were excluded from the PMF modelling. The best solution was obtained with seven

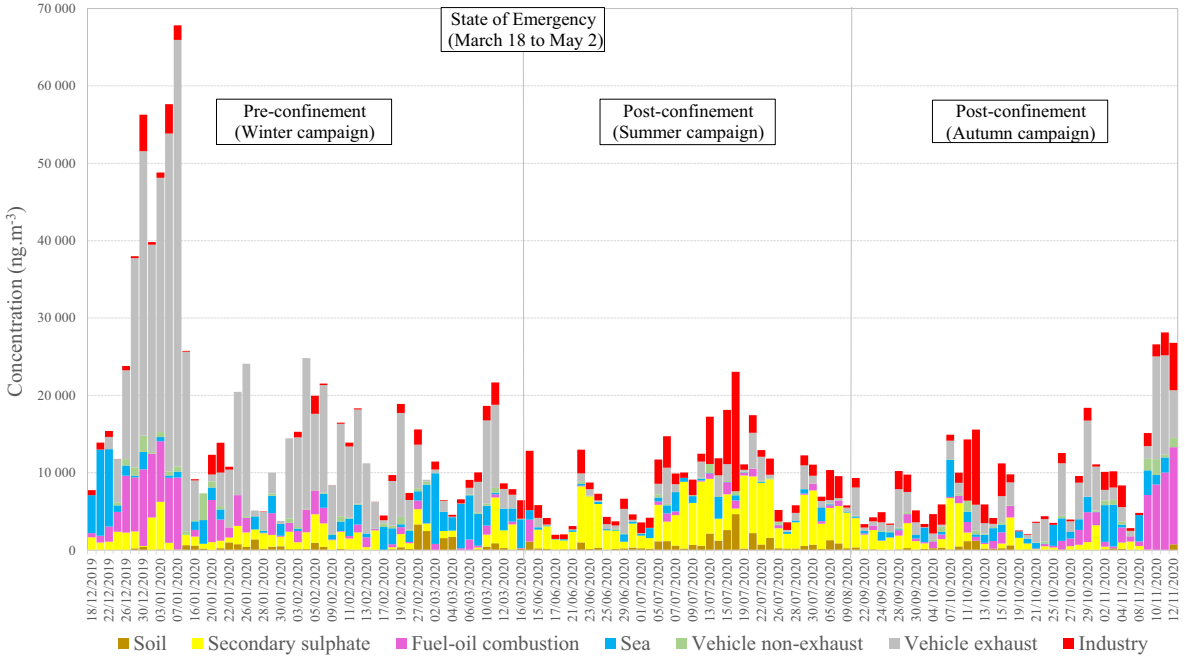

Fig. 5. Source contributions for $PM_{2.5}$ concentrations (ng.m^{-3}) during the sampling period, for the selected PMF solution.

factors. The relation between the modelled and gravimetric $PM_{2.5}$ concentrations (Fig. S8) shows a strong correlation ($r^2 = 0.85$) and slope 0.86, meaning that together the sources accounted for 86% of $PM_{2.5}$. Fig. 4 shows the profiles of the different factors, Fig. 5 presents the source contributions obtained for each sampling day and Fig. 6 provides the source contributions discriminated by sampling campaign.

Factor 1, labelled as "Soil", is defined by Al, Si and Ti, but also with a contribution of Mg and Fe, all typical soil elements (Calvo et al., 2013). This factor contributed on average to 3.6% of $PM_{2.5}$ mass, a value which is relatively low compared to other studies in urban-industrial areas (Silva et al., 2020), but comparable with values found in some coastal urban areas (Manousakas et al., 2017). In fact, it is known that the crustal sources contribute to PM mainly in the coarse mode (>2.5 μm) (Lage et al., 2014; Song and Gao, 2011) and this percentage does not include the contribution of two sampling days when Sahara dust events occurred (Fig. S7).

The contribution of the "Soil" factor was significantly higher in summer/post-confinement/ than in winter/pre-confinement (*p*-value = 0.003) and autumn/post-confinement (p-value = 0.000) (Fig. 6), although there was no significant difference between the pre- and post-confinement periods (p-value >0.050). In fact, Artíñano et al. (2001) indicated that in the Iberian Peninsula there are factors that favour the suspension of dust, especially in summer, such as the dryness and semi-arid soil associated with the high convective

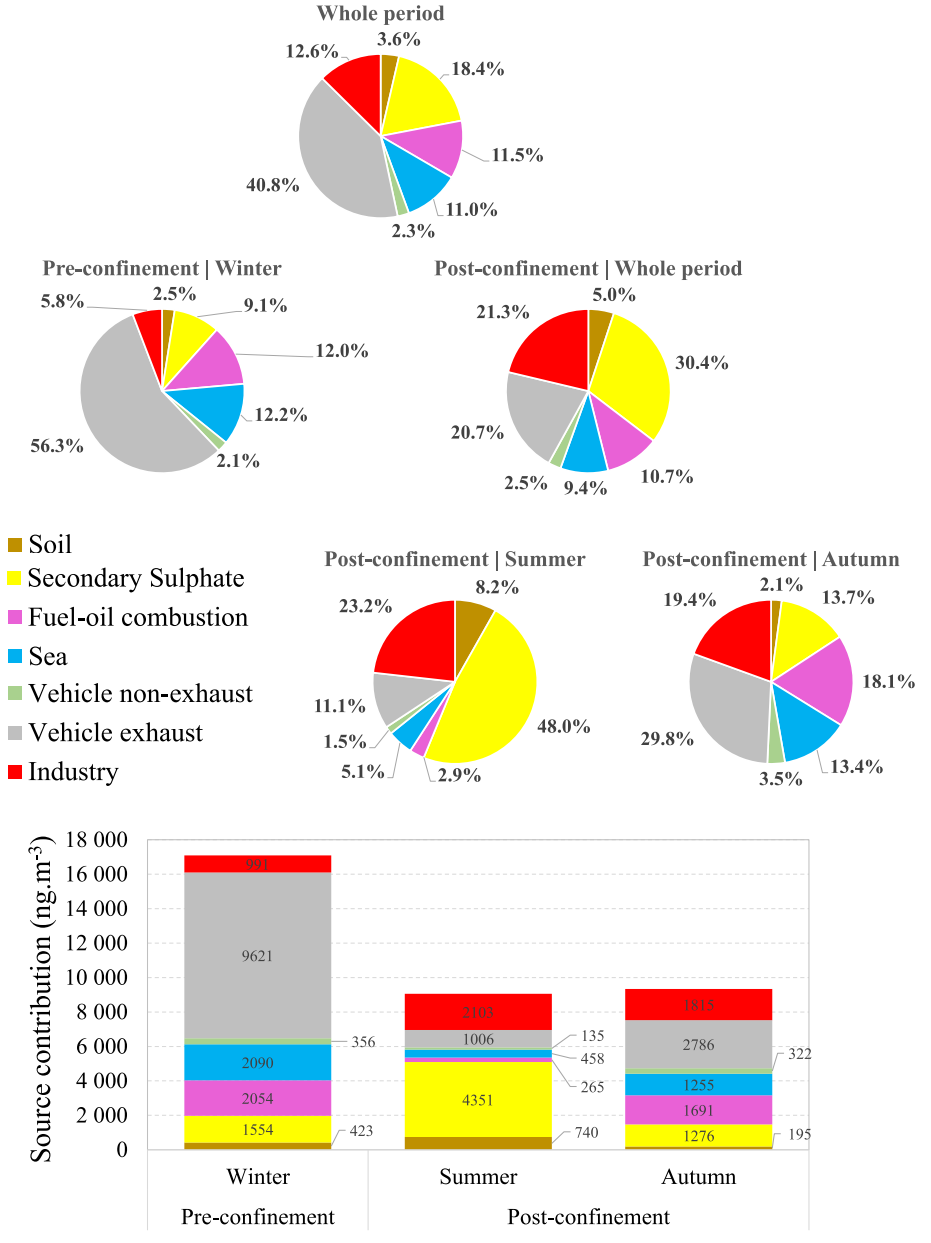

Fig. 6. (top) Relative source contributions for the different sampling periods, and (bottom) source contributions (in $ng.m^{-3}$) for each sampling campaign.

atmospheric dynamics.

Factor 2, which contributed on average to 18.4% of the $PM_{2.5}$ mass, has a chemical profile mainly defined by SO_4^{2-} and NH_4^+, being labelled as "Secondary sulphate", since these ions derive from gas-to-particle conversion processes, from SO_2 oxidation and NH_3 neutralisation (Calvo et al., 2013). In addition to the industry installed in the study area, secondary aerosol certainly also derives from vehicle exhaust emissions, since diesel vehicles are important emitters of sulphates (Calvo et al., 2013). The presence of Na and Mg in the profile may indicate a reaction of SO_2 with sea salt (Salvador et al., 2016).

Furthermore, the profile also includes BC and V contents. A secondary sulphate factor influenced by fuel-oil combustion has been observed in other works (Pey et al., 2013; Titos et al., 2014). In fact, secondary aerosols are not emitted directly into the atmosphere by a single source, resulting from atmospheric chemical transformations of gaseous precursors, at shorter or longer timescales, and therefore they share the same marker species with anthropogenic emissions (Viana et al., 2008). High concentrations of sulphate, V and Ni, especially in the summer season, are also commonly reported in Mediterranean environments associated with re-circulation processes (Pey et al., 2013).

"Secondary sulphate" factor was the major contributor in the post-confinement period, accounting for 30.4% of $PM_{2.5}$ mass and, especially in summer, this factor constituted 48.0% of the aerosol, presenting a significantly higher contribution than in autumn and winter (p-value = 0.000) (Fig. 6). This seasonal pattern was also found in other studies (Pey et al., 2009; Silva et al., 2020). It is due to the enhanced photochemical reactions in summer, and to the fact that higher vehicle emissions in winter and autumn are associated with the preferential formation of NH_4NO_3 at lower temperatures (Almeida et al., 2013) (Fig. S6).

Factor 3 is mainly characterised by V and K. This factor, which contributed to 11.5% of the $PM_{2.5}$ mass, has been labelled as "Fuel-oil combustion", since V is a marker of combustion of heavy oils (Pacyna and Pacyna, 2001). As described in section 2.8., Ni has been considered a "bad" variable and, thus, it was excluded from PMF modelling in this best solution. Nevertheless, in a previous modelling trial when Ni was included (as a "weak" variable), a very similar PMF solution was attained, in which this factor was characterised by V, Ni and K, in a V/Ni ratio of 4.9. Low V/Ni ratios ($\sim$ 0.5) are typically found in diesel combustion particles, while ratios <2 are associated with the presence of a Ni pollution source (Cesari et al., 2014), and ratios of V/Ni between 4 and 5 and ratios of V/EC < 2 are considered tracers of commercial shipping emissions (Pandolfi et al., 2011; Viana et al., 2009). Since in this work, the V/Ni ratio tentative value is 4.9 and V/BC is 0.03, this supports the contribution of ship emissions in the study area, probably due to the proximity from the ferry terminal that connects the two river banks for commuting. Furthermore, this factor also likely represents a mixed industrial combustion source, namely from the petroleum coke combustion in the kiln of the lime industry located in the industrial area of the study site, since V and Ni are also tracers of this combustion (Querol et al., 2007; Viana et al., 2008).

The contribution of the "Fuel-oil combustion" factor was significantly higher in the pre-confinement period (2050 $\pm$ 2740 ng.m^{-3}) than in the post-confinement period (987 $\pm$ 2180 ng.m^{-3}, p-value = 0.003), with no significant difference between winter/pre-confinement/ and autumn/post-confinement (p-value >0.050). In fact, in the confinement and post-confinement periods there was a reduction in the daily number of ferry carriers for commuting between Lisbon and Seixal (Público, 2020), but in autumn this anthropogenic activity had already reached levels similar to the pre-pandemic period.

Factor 4 is labelled as "Sea", given the high contributions of Na, Cl and Mg, typical tracers of sea salt (Calvo et al., 2013). This factor contributed on average to 11.0% of the $PM_{2.5}$ mass, due to the proximity from the Tagus Estuary and the Atlantic Ocean, although the marine aerosol predominantly contributes to the coarse mode (Almeida et al., 2006a; Calvo et al., 2013). The average contribution of this factor (1370 ng.m^{-3}) is similar to the sea salt contribution to $PM_{2.5}$ found in Porto (1220 ng.m^{-3}) (Diapouli et al., 2017).

The average Cl/Na ratio in this factor is 0.98, which is lower than the bulk sea water weight concentration ratio (1.79) (Bowen, 1979). Cl/Na ratios between similar values (1.1) (Almeida et al., 2015) to much lower ones (0.12) (Dall'Osto et al., 2013) have been documented in other works. The discrepancy from the sea water ratio is due to Cl depletion that commonly takes place on urban areas, as a result of the reaction of NaCl with acidic species (HNO_3, SO_2 and H_2SO_4) (Seinfeld and Pandis, 2006). The presence of NO_3^- and SO_4^{2-} in the profile confirms that the sea spray is aged and was subjected to chlorine depletion, with formation of $NaNO_3$ and Na_2SO_4 (Taiwo et al., 2014). The Mg/Na ratio in the factor is 0.12, consistent with the seawater value (0.12) (Seinfeld and Pandis, 2006).

The "Sea" factor presented a significantly higher contribution in winter (p-value = 0.000) and autumn (p-value = 0.011) than in summer (Fig. 6). This can be explained by the higher wave energy in winter and the more intense predominant winds from North (where the Tagus Estuary is located - Fig. 1).

Factor 5 is represented by the elements Zn, Pb, Mn, Cu and Fe. This factor, which accounted for only 2.3% of $PM_{2.5}$ mass, is labelled as "Vehicle non-exhaust", since Zn is a tracer of tyre emissions (Harrison et al., 2012) and Cu, Fe and Zn are markers of brake wear (Grigoratos and Martini, 2015). The elements Pb and Mn are also tracers of brake wear emissions (Lawrence et al., 2013; Song and Gao, 2011). The low contribution of this non-exhaust factor to $PM_{2.5}$ mass may be related to the fact that non-exhaust emissions generally contribute more to coarse particles, while the fine mode particles are mainly derived from combustion (Handler et al., 2008).

The mean contribution of the "Vehicle non-exhaust" factor was significantly higher in winter/pre-confinement than in summer/post-confinement (p-value = 0.047) (Fig. 6), but the difference was not significant between the pre- and post-confinement periods (p-value >0.050).

Factor 6 represents "Vehicle exhaust" and secondary nitrate emissions, due to the high percentage of BC, NO_3^- and NH_4^+ in the factor. In fact, BC can be used as a key tracer of vehicular emissions (Hudda et al., 2020) and NO_3^- derives from NO_x precursors, mainly emitted by fossil fuel combustions, as vehicle exhaust (Arimoto et al., 1996).

In the literature, the presence of total carbon (TC) in secondary inorganic aerosols (SIA) profiles, namely "secondary nitrates" profile, has been assigned to the aging of SIA and/or the effect of mixing with particles from combustion sources, e.g. vehicle exhaust (Kfoury et al., 2016). Koçak et al. (2015) observed a moderate correlation between NO_3^- and TC, the absence of correlation between SO_4^{2-} and TC, and ascribed the NO_3^-–TC relation to the combustion process.

Furthermore, vehicle exhaust is known to contribute to the enrichment of Cu in aerosol particles (Song and Gao, 2011) and this factor indeed accounts for 35.6% of the species. This factor also has a contribution from Pb, corroborating that Pb is also emitted from motor oil combustion (Handler et al., 2008).

Globally, this factor was the main contributor to $PM_{2.5}$ in the study area, accounting for 40.8% of the $PM_{2.5}$ mass, considering the whole period, but this factor presented the most pronounced decrease from the winter/pre-confinement (9620 ± 11,880 ng.m^{-3}) to the post-confinement period (1910 ± 2640 ng.m^{-3}, p-value = 0.000) and its relative contribution to $PM_{2.5}$ mass decreased from 56.3 to 20.7% between the two periods (Fig. 6). These results confirm the relevance of traffic and associated secondary aerosol in $PM_{2.5}$ in the study area and reveal that the decrease in the $PM_{2.5}$ concentrations was due, to a large extent, to the reduction of road traffic. In fact, after the declaration of the state of emergency (on March 18), the volume of traffic during the confinement period decreased drastically to 21% of the volume recorded in January 13, 2020, and then intensified after the end of the state of emergency (May 2). Globally, in the post-confinement period, the volume of traffic in Lisbon Metropolitan Area was on average, 84% of the volume recorded in January 13, 2020 (Apple, 2020).

Factor 7 has high relative contributions of Ca, Fe and Mn, being the main contributor to these elements in $PM_{2.5}$. This factor, which represented 12.6% of $PM_{2.5}$ concentration in the whole period, is labelled as "Industry", since Fe and Mn are tracers of iron and steel industry (Calvo et al., 2013), along with Zn and Pb, which also contribute to the factor. Furthermore, Ca, Fe, Al, Mn and Si are primary constituents of the slag produced in the Electric Arc Furnace (EAF) process, where calcium oxide is added as fluxing agent (Proctor et al., 2000). This association of Fe, Mn and Ca in the same source factor attributed to steelworks emissions was also observed in the vicinity of a major steelworks in the UK and the presence of Ca was also attributed to the use of lime as fluxing agent (Taiwo et al., 2014). It should be mentioned that the EAF steelworks, as the one installed in study area, frequently present fugitive emissions from handling of raw materials, slag processing and dust resuspension (Mohiuddin et al., 2014). This factor presents indeed a character of resuspension, given the significant contribution of crustal elements such as Si and Ti, besides Ca. This factor can also be associated with the lime factory that exists in the industrial area of the study site. It should be mentioned that Fe (32.4%), Ca (26.2%) and Mn (4.62%) were also identified as major components of the settled dust collected in January 2019 in the study area, along with Si (14.9%) and Al (9.67%) (Justino et al., 2019).

While in the winter/pre-confinement period, this factor only represented 5.8% of the $PM_{2.5}$ mass, in the post-confinement period, this factor was one of the main contributors with 21.3% (Fig. 6). In relative terms, this was a consequence of the reduction of "Vehicle exhaust", but the absolute contribution of the "Industry" factor was also significantly higher in the post-confinement (1960 ± 2400 ng.m^{-3}) than in the pre-confinement (991 ± 1439 ng.m^{-3}, p-value = 0.000), probably due to increased resuspension in the dry season and also corroborating the fact that the industries (namely, steelworks) of the study area did not stop to operate during the confinement period (Abecasis et al., 2022).

Globally, these results are in line with other works, where PMF source apportionment generally revealed decreased contributions of vehicle emissions (Cui et al., 2020; Cheng et al., 2022; Wang et al., 2021a) and in some cases, also increased contributions of secondary inorganic aerosol (Chang et al., 2022; Hong et al., 2021; Massimi et al., 2022).

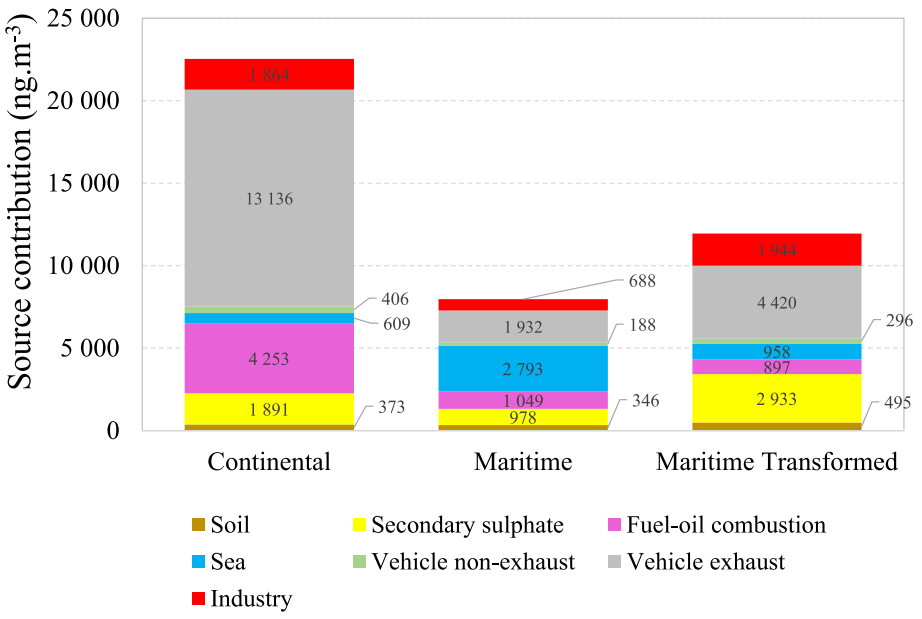

Fig. 7. Source contributions for $PM_{2.5}$ concentrations discriminated by air mass trajectory type.

3.3. Influence of air masses

Since Seixal is at a distance of 12 km from the Atlantic coast, it is influenced by the maritime aerosol, as found for the Lisbon Metropolitan Area (Almeida et al., 2013), with the air mass trajectories of maritime (24%) and maritime transformed (60%) origin predominating in the sampling period (Fig. 2). Lower $PM_{2.5}$ concentrations were determined in maritime clusters (8 ± 5 μg.m^{-3}), followed by maritime-transformed clusters (12 ± 10 μg.m^{-3}), while significantly higher levels were observed for the continental cluster (23 ± 15 μg.m^{-3}, p-value = 0.000). This is expected, since maritime air mass trajectories are usually associated with the transport of cleaner air masses with better dispersion of pollutants (Almeida et al., 2013). Crustal elements Al, Si, Ca, Fe, as well as BC, SO_4^{2-}, NO_3^- and NH_4^+, Mn and Zn, registered significantly higher concentrations (p-value <0.050) in continental and maritime transformed air masses, while as expected, Na, Cl and Mg predominate in maritime air masses (Fig. S9).

The study area was occasionally affected by episodes of dust transport from the North of Africa, which is a phenomenon observed in Portugal and Mediterranean countries (Almeida et al., 2008; Diapouli et al., 2017). Inspecting the time series of the elemental concentrations in the sampling period, peak concentrations were observed in March 18 and July 20 (Fig. S7), for Si (2600 and 2440 ng.m^{-3}), Al (1190 and 1110 ng.m^{-3}), Ca (1070 and 1030 ng.m^{-3}) and Fe (740 and 775 ng.m^{-3}). In these two days, $PM_{2.5}$ concentrations 22 and 20 μg.m^{-3}, and PM_{10} concentrations 42 and 33 μg.m^{-3} were registered, much higher than the mean concentrations of the whole sampling period (13 and 24 μg.m^{-3}, respectively). Backward trajectories by the HYSPLIT model, ending in the sampling site in March 18 and July 20, confirmed the long range transport of air masses from the North of Africa or Southern Europe (Fig. S10), which are usually enriched in soil elements, namely Fe (Almeida et al., 2008). These two days were excluded from PMF modelling and thus do not affect the following conclusions.

The source contributions were calculated for the main types of air mass trajectories. The results presented in Fig. 7 indicate that the different air mass types have influence on the contribution of the emission sources at the receptor. In fact, for maritime and maritime transformed samples, the mean contributions of "Fuel-oil combustion" and "Vehicle exhaust" factors were significantly lower (p-value = 0.000) compared with the samples affected by continental air masses, and as expected, the marine factor contributed significantly more (p-value = 0.000). Maritime transformed air masses present higher contributions than maritime air masses, from "Soil", "Secondary sulphate", "Vehicle non-exhaust" and "Industry" sources (due to the final recirculation through the continent).

4. Conclusions

This study investigated the $PM_{2.5}$ concentrations, composition (including 24 elements, black carbon and secondary inorganic ions) and sources in an urban-industrial area of the Lisbon Metropolitan Area (Seixal), from December 2019 to November 2020, including periods before and after the COVID-19 lockdown.

Source apportionment by PMF yielded seven sources contributing to $PM_{2.5}$ in the study area: soil, secondary sulphate, fuel-oil combustion, sea, vehicle non-exhaust, vehicle exhaust (the main contributor, considering the whole period), and industry. It was concluded that $PM_{2.5}$ concentrations, chemical composition and sources were greatly influenced by the restrictions imposed by the COVID-19 pandemic, with vehicle exhaust presenting the most pronounced decrease. The predominance of secondary sulphate was registered in summer/post-confinement. Besides the restrictions imposed by COVID-19 and the seasonality, the source contributions were affected by the types of air mass trajectories.

The COVID-19 pandemic context offered a unique opportunity to examine the effects of human-related activities on air quality in the study area, helping to define targeted mitigation measures to improve air quality in one of the most air polluted areas of Portugal. This study highlights the need for the priority implementation of traffic reduction measures, through better planning of the metropolitan area, creation of an efficient and high interconnectivity public transport network, incentives to the population for the use of public transport and electric mobility, and stimulation of teleworking, in order to reduce commuting movements. Industry measures are also needed to mitigate fugitive emissions. Secondary aerosol and its underlying factors deserve a special attention and need further research in the study area.

Author statement

The roles of each author in the submitted manuscript are the following:

C.A.G., A.S. and S.B. performed the filter sampling.

Z.K. performed the chemical analysis by PIXE.

A.V. and C.A. performed the ions chemical analysis.

C.A.G. performed the black carbon analysis.

C.A.G. performed the formal analysis, data curation and analysis, including statistical and modelling.

C.A.G. and N.C. wrote the original draft.

S.M.A., C.A. and N.C. reviewed the manuscript.

S.M.A. was responsible for the conceptualization, scientific supervision, review of the manuscript, funding acquisition, coordination of the project.

All authors have read and agreed to the published version of the manuscript.

Declaration of Competing Interest

The authors declare that they have no known competing financial interests or personal relationships that could have appeared to influence the work reported in this paper.

Data availability

Data will be made available on request.

Acknowledgements

Acknowledgements are due to Câmara Municipal do Seixal and UFSAAPP, for funding and all the support given in the sampling process. The PIXE measurements were supported by the grant GINOP-2.3.3-15-2016-00029. N. Canha acknowledges the support by national funds through FCT-Fundação para a Ciência e Tecnologia, I.P. (Portugal) for his contract 2021.00088.CEECIND. Ana Vicente was subsidised by national funds (OE), through FCT, I.P., in the framework contract foreseen in the numbers 4, 5 and 6 of article 23, of the Decree-Law 57/2016, of August 29, changed by Law 57/2017, of July 19. The financial support to C^2TN/IST (UIDB/04349/2020 + UIDP/04349/2020) and CESAM (UIDP/50017/2020 + UIDB/50017/2020 + LA/P/0094/2020) by FCT/MCTES, through national funds, is also acknowledged. The authors would also like to thank the Instituto Português do Mar e da Atmosfera (IPMA) for providing the meteorological data.

Appendix A. Supplementary data

Supplementary data to this article can be found online at https://doi.org/10.1016/j.uclim.2023.101446.

References

Abecasis, L., Gamelas, C.A., Justino, A.R., Dionísio, I., Canha, N., Kertesz, Z., Almeida, S.M., 2022. Spatial distribution of air pollution, hotspots and sources in an urban-industrial area in the Lisbon metropolitan area, Portugal—a biomonitoring approach. Int. J. Environ. Res. Public Health 19, 1364. https://doi.org/10.3390/ijerph19031364.

Aix, M.L., Petit, P., Bicout, D.J., 2022. Air pollution and health impacts during the COVID-19 lockdowns in Grenoble, France. Environ. Pollut. 303, 119134 https://doi.org/10.1016/j.envpol.2022.119134.

Almeida, S.M., Freitas, M.C., Reis, M.A., Pio, C.A., Trancoso, M.A., 2006a. Combined application of multielement analysis-k0-INAA and PIXE-and classical techniques for source apportionment in aerosol studies. Nucl. Instru. Methods Phys. Res. Sect. A Accel. Spectrometers Detect. Assoc. Equip. 564, 752–760. https://doi.org/10.1016/j.nima.2006.04.007.

Almeida, S.M., Pio, C.A., Freitas, M.C., Reis, M.A., Trancoso, M.A., 2006b. Source apportionment of atmospheric urban aerosol based on weekdays/weekend variability: evaluation of road re-suspended dust contribution. Atmos. Environ. 40, 2058–2067. https://doi.org/10.1016/j.atmosenv.2005.11.046.

Aljboor, S., Angyal, A., Papp, E., Baranyai, D., Papp, E., Szarka, M., Szikszai, Z., Rajta, I., Vajda, I., Kertész, Z., 2023. Light-element sensitive in-air millibeam PIXE setup for fast measurement of atmospheric aerosol samples. J. Anal. At. Spectrom. 38, 57–65. https://doi.org/10.1039/d2ja00291d.

Almeida, S.M., Freitas, M.C., Pio, C.A., 2008. Neutron activation analysis for identification of African mineral dust transport. J. Radioanal. Nucl. Chem. 276, 161–165. https://doi.org/10.1007/s10967-007-0426-4.

Almeida, S.M., Ramos, C.A., Marques, A.M., Silva, A.V., Freitas, M.C., Farinha, M.M., Reis, M., Marques, A.P., 2012. Use of INAA and PIXE for multipollutant air quality assessment and management. J. Radioanal. Nucl. Chem. 294, 343–347. https://doi.org/10.1007/s10967-011-1473-4.

Almeida, S.M., Silva, A.I., Freitas, M.C., Dzung, H.M., Caseiro, A., Pio, C.A., 2013. Impact of maritime air mass trajectories on the western european coast urban aerosol. J. Toxicol. Environ. Heal. - Part A Curr. Issues 76, 252–262. https://doi.org/10.1080/15287394.2013.757201.

Almeida, S.M., Lage, J., Fernández, B., Garcia, S., Reis, M.A., Chaves, P.C., 2015. Chemical characterization of atmospheric particles and source apportionment in the vicinity of a steelmaking industry. Sci. Total Environ. 521–522, 411–420. https://doi.org/10.1016/j.scitotenv.2015.03.112.

Almeida, S.M., Manousakas, M., Diapouli, E., Kertesz, Z., Samek, L., Hristova, E., Šega, K., Alvarez, R.P., Belis, C.A., Eleftheriadis, K., Albania Civici, N., Radic, R., Vukic, L., Hristova, E., Veleva, B., Šega, K., Bešlic, I., Davila, S., Godec, R., Manousakas, M., Diapouli, E., Vratolis, S., Eleftheriadis, K., Kertesz, Z., Belis, C.A., Bernatonis, M., Djukanovic, G., Jancic, D., Samek, L., Furman, L., Stegowski, Z., Almeida, S.M., Galinha, C., Balan, V., Nikolovska, L., Stefanovska, A., Radenkovic, M., Kneževic, J., Banu Oztas, N., Cantay, E., Turchenko, D.V., Abdullaev, S., Padilla Alvarez, R., Karydas, A.G., 2020. Ambient particulate matter source apportionment using receptor modelling in European and Central Asia urban areas. Environ. Pollut. 266 https://doi.org/10.1016/j.envpol.2020.115199.

Almeida-Silva, M., Canha, N., Vogado, F., Baptista, P.C., Faria, A.V., Faria, T., Coutinho, J.T., Alves, C., Almeida, S.M., 2020. Assessment of particulate matter levels and sources in a street canyon at Loures, Portugal – a case study of the REMEDIO project. Atmos. Pollut. Res. 11, 1857–1869. https://doi.org/10.1016/j.apr.2020.07.021.

Amato, F., Pandolfi, M., Escrig, A., Querol, X., Alastuey, A., Pey, J., Perez, N., Hopke, P.K., 2009. Quantifying road dust resuspension in urban environment by multilinear engine: a comparison with PMF2. Atmos. Environ. 43, 2770–2780. https://doi.org/10.1016/j.atmosenv.2009.02.039.

Amato, F., Alastuey, A., Karanasiou, A., Lucarelli, F., Nava, S., Calzolai, G., Severi, M., Becagli, S., Gianelle, V.L., Colombi, C., Alves, C., Custódio, D., Nunes, T., Cerqueira, M., Pio, C., Eleftheriadis, K., Diapouli, E., Reche, C., Minguillón, M.C., Manousakas, M.I., Maggos, T., Vratolis, S., Harrison, R.M., Querol, X., 2016. AIRUSE-LIFE+: a harmonized PM speciation and source apportionment in five southern European cities. Atmos. Chem. Phys. 16, 3289–3309. https://doi.org/10.5194/acp-16-3289-2016.

APA - Portuguese Environmental Agency, 2022. APA QualAR - National Air Quality Monitoring Network [WWW Document]. URL. https://qualar.apambiente.pt/ (accessed 2.13.22).

Apple, 2020. Apple mobility trend reports [WWW Document]. URL. https://covid19.apple.com/mobility (accessed 2.13.22).

Arimoto, R., Duce, R.A., Savoie, D.L., Prospero, J.M., Talbot, R., Cullen, J.D., Tomza, U., Lewis, N.F., Ray, B.J., 1996. Relationships among aerosol constituents from Asia and the North Pacific during PEM-west a. J. Geophys. Res. 101, 2011–2023.

Artíñano, B., Querol, X., Salvador, P., Rodríguez, S., Alonso, D.G., Alastuey, A., 2001. Assessment of airborne particulate levels in Spain in relation to the new EU-directive. Atmos. Environ. 35, 43–53. https://doi.org/10.1016/s1352-2310(00)00467-2.

Assembleia da República, 2021. Estado de Emergência - Declarações e Relatórios [WWW Document]. URL. https://www.parlamento.pt/Paginas/estado-emergencia.aspx (accessed 2.13.22).
Balamurugan, V., Chen, J., Qu, Z., Bi, X., Keutsch, F.N., 2022. Secondary PM2.5 decreases significantly less than NO2 emission reductions during COVID lockdown in Germany. Atmos. Chem. Phys. 22, 7105–7129. https://doi.org/10.5194/acp-22-7105-2022.
Belis, C.A., Karagulian, F., Larsen, B.R., Hopke, P.K., 2013. Critical review and meta-analysis of ambient particulate matter source apportionment using receptor models in Europe. Atmos. Environ. https://doi.org/10.1016/j.atmosenv.2012.11.009.
Bowen, H.J.M., 1979. Environmental Chemistry of the Elements. Academic Press, London.
Cai, F., Yin, K., Hao, M., 2022. COVID-19 pandemic, air quality, and PM2.5 reduction-induced health benefits: a comparative study for three significant periods in Beijing. Front. Ecol. Evol. 10 https://doi.org/10.3389/fevo.2022.885955.
Cakmak, S., Dales, R., Kauri, L.M., Mahmud, M., Van Ryswyk, K., Vanos, J., Liu, L., Kumarathasan, P., Thomson, E., Vincent, R., Weichenthal, S., 2014. Metal composition of fine particulate air pollution and acute changes in cardiorespiratory physiology. Environ. Pollut. 189, 208–214. https://doi.org/10.1016/j.envpol.2014.03.004.
Calvo, A.I., Alves, C., Castro, A., Pont, V., Vicente, A.M., Fraile, R., 2013. Research on aerosol sources and chemical composition: past, current and emerging issues. Atmos. Res. https://doi.org/10.1016/j.atmosres.2012.09.021.
Campbell, J.L., Boyd, N.I., Grassi, N., Bonnick, P., Maxwell, J.A., 2010. The Guelph PIXE software package IV. Nucl. Instru. Methods Phys. Res. Sect B Beam Interact. with Mater. Atoms 268, 3356–3363. https://doi.org/10.1016/j.nimb.2010.07.012.
Cesari, D., Genga, A., Ielpo, P., Siciliano, M., Mascolo, G., Grasso, F.M., Contini, D., 2014. Source apportionment of PM2.5 in the harbour-industrial area of Brindisi (Italy): identification and estimation of the contribution of in-port ship emissions. Sci. Total Environ. 497–498, 392–400. https://doi.org/10.1016/j.scitotenv.2014.08.007.
Chang, Y., Huang, R., Ge, X., Huang, X., Hu, J., Duan, Y., Zou, Z., Liu, X., Lehmann, M.F., 2020. Puzzling haze events in China during the coronavirus (COVID-19) shutdown. Geophys. Res. Lett. 47 https://doi.org/10.1029/2020GL088533.
Chang, Y., Du, T., Song, X., Wang, W., Tian, P., Guan, X., Zhang, N., 2022. Changes in physical and chemical properties of urban atmospheric aerosols and ozone during the COVID-19 lockdown in a semi-arid region. Atmos. Environ. 287, 119270 https://doi.org/10.1016/j.atmosenv.2022.119270.
Chauhan, A., Singh, R.P., 2020. Decline in PM 2.5 concentrations over major cities around the world associated with COVID-19. Environ. Res. 187, 109634 https://doi.org/10.1016/j.envres.2020.109634.
Chen, H., Huo, J., Fu, Q., Duan, Y., Xiao, H., Chen, J., 2020a. Impact of quarantine measures on chemical compositions of PM2.5 during the COVID-19 epidemic in Shanghai, China. Sci. Total Environ. 743, 140758 https://doi.org/10.1016/j.scitotenv.2020.140758.
Chen, Y., Zhang, S., Peng, C., Shi, G., Tian, M., Huang, R.J., Guo, D., Wang, H., Yao, X., Yang, F., 2020b. Impact of the COVID-19 pandemic and control measures on air quality and aerosol light absorption in southwestern China. Sci. Total Environ. 749, 141419 https://doi.org/10.1016/j.scitotenv.2020.141419.
Cheng, K., Chang, Y., Kuang, Y., Khan, R., Zou, Z., 2022. Elucidating the responses of highly time-resolved PM2.5 related elements to extreme emission reductions. Environ. Res. 206, 112624 https://doi.org/10.1016/j.envres.2021.112624.
Collivignarelli, M.C., Abbà, A., Bertanza, G., Pedrazzani, R., Ricciardi, P., Carnevale Miino, M., 2020. Lockdown for CoViD-2019 in Milan: what are the effects on air quality? Sci. Total Environ. 732, 139280 https://doi.org/10.1016/j.scitotenv.2020.139280.
Cui, Y., Ji, D., Maenhaut, W., Gao, W., Zhang, R., Wang, Y., 2020. Levels and sources of hourly PM2.5-related elements during the control period of the COVID-19 pandemic at a rural site between Beijing and Tianjin. Sci. Total Environ. 744, 140840 https://doi.org/10.1016/j.scitotenv.2020.140840.
Dall'Osto, M., Querol, X., Amato, F., Karanasiou, A., Lucarelli, F., Nava, S., Calzolai, G., Chiari, M., 2013. Hourly elemental concentrations in PM2.5 aerosols sampled simultaneously at urban background and road site during SAPUSS -diurnal variations and PMF receptor modelling. Atmos. Chem. Phys. 13, 4375–4392. https://doi.org/10.5194/acp-13-4375-2013.
Diapouli, E., Manousakas, M.I., Vratolis, S., Vasilatou, V., Pateraki, S., Bairachtari, K.A., Querol, X., Amato, F., Alastuey, A., Karanasiou, A.A., Lucarelli, F., Nava, S., Calzolai, G., Gianelle, V.L., Colombi, C., Alves, C., Custódio, D., Pio, C., Spyrou, C., Kallos, G.B., Eleftheriadis, K., 2017. AIRUSE-LIFE +: estimation of natural source contributions to urban ambient air PM10 and PM2. 5 concentrations in southern Europe - implications to compliance with limit values. Atmos. Chem. Phys. 17, 3673–3685. https://doi.org/10.5194/acp-17-3673-2017.
Eeftens, M., Tsai, M.Y., Ampe, C., Anwander, B., Beelen, R., Bellander, T., Cesaroni, G., Cirach, M., Cyrys, J., de Hoogh, K., De Nazelle, A., de Vocht, F., Declercq, C., Dedele, A., Eriksen, K., Galassi, C., Gražulevičiene, R., Grivas, G., Heinrich, J., Hoffmann, B., Iakovides, M., Ineichen, A., Katsouyanni, K., Korek, M., Krämer, U., Kuhlbusch, T., Lanki, T., Madsen, C., Meliefste, K., Mölter, A., Mosler, G., Nieuwenhuijsen, M., Oldenwening, M., Pennanen, A., Probst-Hensch, N., Quass, U., Raaschou-Nielsen, O., Ranzi, A., Stephanou, E., Sugiri, D., Udvardy, O., Vaskövi, É., Weinmayr, G., Brunekreef, B., Hoek, G., 2012. Spatial variation of PM2.5, PM10, PM2.5 absorbance and PMcoarse concentrations between and within 20 European study areas and the relationship with NO2 - results of the ESCAPE project. Atmos. Environ. 62, 303–317. https://doi.org/10.1016/j.atmosenv.2012.08.038.
European Environmental Agency, 2020. Air Quality in Europe - 2020 Report, EEA Report.
Faria, T., Martins, V., Correia, C., Canha, N., Diapouli, E., Manousakas, M., Eleftheriadis, K., Almeida, S.M., 2020. Children's exposure and dose assessment to particulate matter in Lisbon. Build. Environ. 171, 106666 https://doi.org/10.1016/j.buildenv.2020.106666.
Fatima, S., Ahlawat, A., Mishra, S.K., Maheshwari, M., Soni, V.K., 2022. Variations and source apportionment of PM2.5 and PM10 before and during COVID-19 lockdown phases in Delhi, India. Mapan - J. Metrol. Soc. India. https://doi.org/10.1007/s12647-021-00506-5.
Gama, C., Relvas, H., Lopes, M., Monteiro, A., 2021. The impact of COVID-19 on air quality levels in Portugal: a way to assess traffic contribution. Environ. Res. 193 https://doi.org/10.1016/j.envres.2020.110515.
Gamelas, C., Abecasis, L., Canha, N., Almeida, S.M., 2021. The impact of COVID-19 confinement measures on the air quality in an urban-industrial area of Portugal. Atmosphere (Basel). 12, 1097. https://doi.org/10.3390/atmos12091097.
Gao, Y., Guo, X., Ji, H., Li, C., Ding, H., Briki, M., Tang, L., Zhang, Y., 2016. Potential threat of heavy metals and PAHs in PM2.5 in different urban functional areas of Beijing. Atmos. Res. 178–179, 6–16. https://doi.org/10.1016/j.atmosres.2016.03.015.
Granados-Muñoz, M.J., Navas-Guzmán, F., Bravo-Aranda, J.A., Guerrero-Rascado, J.L., Lyamani, H., Fernández-Gálvez, J., Alados-Arboledas, L., 2012. Automatic determination of the planetary boundary layer height using lidar: One-year analysis over southeastern Spain. J. Geophys. Res. Atmos. 117.
Grigoratos, T., Martini, G., 2015. Brake wear particle emissions: a review. Environ. Sci. Pollut. Res. 22, 2491–2504. https://doi.org/10.1007/s11356-014-3696-8.
Handler, M., Puls, C., Zbiral, J., Marr, I., Puxbaum, H., Limbeck, A., 2008. Size and composition of particulate emissions from motor vehicles in the Kaisermühlentunnel, Vienna. Atmos. Environ. 42, 2173–2186. https://doi.org/10.1016/j.atmosenv.2007.11.054.
Harrison, R.M., Yin, J., 2000. Particulate matter in the atmosphere: which particle properties are important for its effects on health? Sci. Total Environ. 249, 85–101. https://doi.org/10.1016/S0048-9697(99)00513-6.
Harrison, R.M., Jones, A.M., Gietl, J., Yin, J., Green, D.C., 2012. Estimation of the contributions of brake dust, tire wear, and resuspension to nonexhaust traffic particles derived from atmospheric measurements. Environ. Sci. Technol. 46, 6523–6529. https://doi.org/10.1021/es300894r.
He, G., Pan, Y., Tanaka, T., 2020. The short-term impacts of COVID-19 lockdown on urban air pollution in China. Nat. Sustain. 3, 1005–1011. https://doi.org/10.1038/s41893-020-0581-y.
Healy, R.M., Sofowote, U., Su, Y., Debosz, J., Noble, M., Jeong, C.H., Wang, J.M., Hilker, N., Evans, G.J., Doerksen, G., Jones, K., Munoz, A., 2017. Ambient measurements and source apportionment of fossil fuel and biomass burning black carbon in Ontario. Atmos. Environ. 161, 34–47. https://doi.org/10.1016/j.atmosenv.2017.04.034.
Hicks, W., Beevers, S., Tremper, A.H., Stewart, G., Priestman, M., Kelly, F.J., Lanoisellé, M., Lowry, D., Green, D.C., 2021. Quantification of non-exhaust particulate matter traffic emissions and the impact of COVID-19 lockdown at London Marylebone road. Atmosphere (Basel). 12, 190. https://doi.org/10.3390/atmos12020190.
Hong, Y., Xu, X., Liao, D., Zheng, R., Ji, X., Chen, Y., Xu, L., Li, M., Wang, H., Xiao, H., Choi, S.D., Chen, J., 2021. Source apportionment of PM2.5 and sulfate formation during the COVID-19 lockdown in a coastal city of Southeast China. Environ. Pollut. 286, 117577 https://doi.org/10.1016/j.envpol.2021.117577.

Hudda, N., Simon, M.C., Patton, A.P., Durant, J.L., 2020. Reductions in traffic-related black carbon and ultrafine particle number concentrations in an urban neighborhood during the COVID-19 pandemic. Sci. Total Environ. 742, 140931 https://doi.org/10.1016/j.scitotenv.2020.140931.

Justino, A.R.R., Canha, N., Gamelas, C., Coutinho, J.T.T., Kertesz, Z., Almeida, S.M.M., 2019. Contribution of micro-PIXE to the characterization of settled dust events in an urban area affected by industrial activities. J. Radioanal. Nucl. Chem. 322, 1953–1964. https://doi.org/10.1007/s10967-019-06860-8.

Kfoury, A., Ledoux, F., Roche, C., Delmaire, G., Roussel, G., Courcot, D., 2016. PM2.5 source apportionment in a French urban coastal site under steelworks emission influences using constrained non-negative matrix factorization receptor model. J. Environ. Sci. (China) 40, 114–128. https://doi.org/10.1016/j.jes.2015.10.025.

Kim, K.H., Kabir, E., Kabir, S., 2015. A review on the human health impact of airborne particulate matter. Environ. Int. 74, 136–143. https://doi.org/10.1016/j.envint.2014.10.005.

Koçak, M., Mihalopoulos, N., Tutsak, E., Theodosi, C., Zarmpas, P., Kalegeri, P., 2015. PM10 and PM2.5 composition over the Central Black Sea: origin and seasonal variability. Environ. Sci. Pollut. Res. 22, 18076–18092. https://doi.org/10.1007/s11356-015-4928-2.

Lage, J., Almeida, S.M., Reis, M.A., Chaves, P.C., Ribeiro, T., Garcia, S., Faria, J.P., Fernández, B.G., Wolterbeek, H.T., 2014. Levels and spatial distribution of airborne chemical elements in a heavy industrial area located in the north of Spain. J. Toxicol. Environ. Heal. - Part A Curr. Issues 77, 856–866. https://doi.org/10.1080/15287394.2014.910156.

Lage, J., Wolterbeek, H.T., Reis, M.A., Chaves, P.C., Garcia, S., Almeida, S.M., 2016. Source apportionment by positive matrix factorization on elemental concentration obtained in PM10 and biomonitors collected in the vicinities of a steelworks. J. Radioanal. Nucl. Chem. 309, 397–404. https://doi.org/10.1007/s10967-016-4751-3.

Lawrence, S., Sokhi, R., Ravindra, K., Mao, H., Prain, H.D., Bull, I.D., 2013. Source apportionment of traffic emissions of particulate matter using tunnel measurements. Atmos. Environ. 77, 548–557. https://doi.org/10.1016/j.atmosenv.2013.03.040.

Li, R., Zhao, Y., Fu, H., Chen, J., Peng, M., Wang, C., 2021. Substantial changes in gaseous pollutants and chemical compositions in fine particles in the North China plain during the COVID-19 lockdown period: anthropogenic vs. meteorological influences. Atmos. Chem. Phys. 21, 8677–8692. https://doi.org/10.5194/acp-21-8677-2021.

Liu, W., Mao, Y., Hu, T., Shi, M., Zhang, J., Zhang, Y., 2022. Variation of pollution sources and health effects on air pollution before and during COVID-19 pandemic in Linfen, Fenwei Plain. Environ. Res. 113719 https://doi.org/10.1016/j.envres.2022.113719.

Lyamani, H., Fernández-Gálvez, J., Pérez-Ramírez, D., Valenzuela, A., Antón, M., Alados, I., Titos, G., Olmo, F.J., Alados-Arboledas, L., 2012. Aerosol properties over two urban sites in South Spain during an extended stagnation episode in winter season. Atmos. Environ. 62, 424–432. https://doi.org/10.1016/j.atmosenv.2012.08.050.

Ma, T., Duan, F., Ma, Y., Zhang, Q., Xu, Y., Li, W., Zhu, L., He, K., 2022. Unbalanced emission reductions and adverse meteorological conditions facilitate the formation of secondary pollutants during the COVID-19 lockdown in Beijing. Sci. Total Environ. 155970 https://doi.org/10.1016/j.scitotenv.2022.155970.

Manohar, M., Atanacio, A., Button, D., Cohen, D., 2021. MABI - a multi-wavelength absorption black carbon instrument for the measurement of fine light absorbing carbon particles. Atmos. Pollut. Res. 12, 133–140. https://doi.org/10.1016/j.apr.2021.02.009.

Manousakas, M., Papaefthymiou, H., Diapouli, E., Migliori, A., Karydas, A.G., Bogdanovic-Radovic, I., Eleftheriadis, K., 2017. Assessment of PM2.5 sources and their corresponding level of uncertainty in a coastal urban area using EPA PMF 5.0 enhanced diagnostics. Sci. Total Environ. 574, 155–164. https://doi.org/10.1016/j.scitotenv.2016.09.047.

Massimi, L., Pietrodangelo, A., Frezzini, M.A., Ristorini, M., De Francesco, N., Sargolini, T., Amoroso, A., Di Giosa, A., Canepari, S., Perrino, C., 2022. Effects of COVID-19 lockdown on PM10 composition and sources in the Rome area (Italy) by elements' chemical fractionation-based source apportionment. Atmos. Res. 266, 105970 https://doi.org/10.1016/j.atmosres.2021.105970.

Mohiuddin, K., Strezov, V., Nelson, P.F., Stelcer, E., 2014. Characterisation of trace metals in atmospheric particles in the vicinity of iron and steelmaking industries in Australia. Atmos. Environ. 83, 72–79. https://doi.org/10.1016/j.atmosenv.2013.11.011.

Nguyen, T.P., Bui, T., Nguyen, M., Nguyen, T.H., Vu, V., Pham, H., 2022. Impact of Covid-19 partial lockdown on PM2.5, SO2, NO2, O3, and trace elements in PM2.5 in Hanoi, Vietnam. Environ. Sci. Pollut. Res. 29, 41875–41885. https://doi.org/10.1007/s11356-021-13792-y.

Paatero, P., 1999. The multilinear engine—a table-driven, least squares program for solving multilinear problems, including the n-way parallel factor analysis model. J. Comput. Graph. Stat. 8, 854–888. https://doi.org/10.1080/10618600.1999.10474853.

Paatero, P., Eberly, S., Brown, S.G., Norris, G.A., 2014. Methods for estimating uncertainty in factor analytic solutions. Atmos. Meas. Tech. 7, 781–797. https://doi.org/10.5194/amt-7-781-2014.

Pacyna, J.M., Pacyna, E.G., 2001. An assessment of global and regional emissions of trace metals to the atmosphere from anthropogenic sources worldwide. Environ. Rev. 9, 269–298. https://doi.org/10.1139/er-9-4-269.

Pandolfi, M., Gonzalez-Castanedo, Y., Alastuey, A., de la Rosa, J.D., Mantilla, E., de la Campa, A.S., Querol, X., Pey, J., Amato, F., Moreno, T., 2011. Source apportionment of PM10 and PM2.5 at multiple sites in the strait of Gibraltar by PMF: impact of shipping emissions. Environ. Sci. Pollut. Res. 18, 260–269. https://doi.org/10.1007/s11356-010-0373-4.

Pey, J., Pérez, N., Castillo, S., Viana, M., Moreno, T., Pandolfi, M., López-Sebastián, J.M., Alastuey, A., Querol, X., 2009. Geochemistry of regional background aerosols in the Western Mediterranean. Atmos. Res. 94, 422–435. https://doi.org/10.1016/j.atmosres.2009.07.001.

Pey, J., Alastuey, A., Querol, X., 2013. PM10 and PM2.5 sources at an insular location in the western mediterranean by using source apportionment techniques. Sci. Total Environ. 456–457, 267–277. https://doi.org/10.1016/j.scitotenv.2013.03.084.

PORDATA, 2022. Base de Dados Portugal Contemporâneo [WWW Document]. URL. http://www.pordata.pt/Municipios/Ambiente+de+%0AConsulta/Tabela (accessed 2.13.22).

Presidência da República, 2020. Decreto do Presidente da República 14-A/2020 de 18 de março. Diário da República n.o 55/2020, 3o Suplemento, Série I, 2, 13-(2)-13-(4). [WWW Document]. URL. https://dre.pt/web/guest/home/-/dre/130399862/details/maximized.

Proctor, D.M., Fehling, K.A., Shay, E.C., Wittenborn, J.L., Green, J.J., Avent, C., Bigham, R.D., Connolly, M., Lee, B., Shepker, T.O., Zak, M.A., 2000. Physical and chemical characteristics of blast furnace, basic oxygen furnace, and electric arc furnace steel industry slags. Environ. Sci. Technol. 34, 1576–1582. https://doi.org/10.1021/es9906002.

Público, 2020. Utentes da Transtejo protestam na Trafaria contra redução de horários das carreiras [WWW Document]. URL. https://www.publico.pt/2020/07/07/local/noticia/utentes-transtejo-protestam-trafaria-reducao-horarios-carreiras-1923345?msclkid=d06ac0d6af8b11ec9a459503e7c6a546.

Putaud, J.P., Van Dingenen, R., Alastuey, A., Bauer, H., Birmili, W., Cyrys, J., Flentje, H., Fuzzi, S., Gehrig, R., Hansson, H.C., Harrison, R.M., Herrmann, H., Hitzenberger, R., Hüglin, C., Jones, A.M., Kasper-Giebl, A., Kiss, G., Kousa, A., Kuhlbusch, T.A.J., Löschau, G., Maenhaut, W., Molnar, A., Moreno, T., Pekkanen, J., Perrino, C., Pitz, M., Puxbaum, H., Querol, X., Rodriguez, S., Salma, I., Schwarz, J., Smolik, J., Schneider, J., Spindler, G., ten Brink, H., Tursic, J., Viana, M., Wiedensohler, A., Raes, F., 2010. A European aerosol phenomenology - 3: physical and chemical characteristics of particulate matter from 60 rural, urban, and kerbside sites across Europe. Atmos. Environ. 44, 1308–1320. https://doi.org/10.1016/j.atmosenv.2009.12.011.

Querol, X., Viana, M., Alastuey, A., Amato, F., Moreno, T., Castillo, S., Pey, J., De Rosa, J., Sa, A., Salvador, P., Santamarı, J.M., Zabalza, J., 2007. Source origin of trace elements in PM from regional background, urban and industrial sites of Spain. Atmos. Environ. 41, 7219–7231. https://doi.org/10.1016/j.atmosenv.2007.05.022.

Querol, X., Massagué, J., Alastuey, A., Moreno, T., Gangoiti, G., Mantilla, E., Duéguez, J.J., Escudero, M., Monfort, E., Pérez García-Pando, C., Petetin, H., Jorba, O., Vázquez, V., de la Rosa, J., Campos, A., Muñóz, M., Monge, S., Hervás, M., Javato, R., Cornide, M.J., 2021. Lessons from the COVID-19 air pollution decrease in Spain: now what? Sci. Total Environ. 779 https://doi.org/10.1016/j.scitotenv.2021.146380.

Rajta, I., Vajda, I., Gyürky, G., Csedreki, L., Kiss, Z., Biri, S., van Oosterhout, H.A.P., Podaru, N.C., Mous, D.J.W., 2018. Accelerator characterization of the new ion beam facility at MTA Atomki in Debrecen, Hungary. Nucl. Instru. Methods Phys. Res. Sect. A Accel. Spectrometers Detect. Assoc. Equip. 880, 125–130. https://doi.org/10.1016/j.nima.2017.10.073.

Rodríguez-Urrego, D., Rodríguez-Urrego, L., 2020. Air quality during the COVID-19: PM2.5 analysis in the 50 most polluted capital cities in the world. Environ. Pollut. 266, 115042 https://doi.org/10.1016/j.envpol.2020.115042.

Salvador, P., Almeida, S.M., Cardoso, J., Almeida-Silva, M., Nunes, T., Cerqueira, M., Alves, C., Reis, M.A., Chaves, P.C., Artíñano, B., Pio, C., 2016. Composition and origin of PM10 in Cape Verde: characterization of long-range transport episodes. Atmos. Environ. 127, 326–339. https://doi.org/10.1016/j.atmosenv.2015.12.057.

Seinfeld, J.H., Pandis, S.N., 2006. Atmospheric Chemistry and Physics - from Air Pollution to Climate Change. John Wiley.

Sharma, S., Zhang, M., Anshika Gao, J., Zhang, H., Kota, S.H., 2020. Effect of restricted emissions during COVID-19 on air quality in India. Sci. Total Environ. 728, 138878 https://doi.org/10.1016/j.scitotenv.2020.138878.

Silva, A.V., Oliveira, C.M., Canha, N., Miranda, A.I., Almeida, S.M., 2020. Long-term assessment of air quality and identification of aerosol sources at Setúbal, Portugal. Int. J. Environ. Res. Public Health 17, 5447. https://doi.org/10.3390/ijerph17155447.

Song, F., Gao, Y., 2011. Size distributions of trace elements associated with ambient particular matter in the affinity of a major highway in the New Jersey-New York metropolitan area. Atmos. Environ. 45, 6714–6723. https://doi.org/10.1016/j.atmosenv.2011.08.031.

Stein, A.F., Draxler, R.R., Rolph, G.D., Stunder, B.J.B., Cohen, M.D., Ngan, F., 2015. NOAA's hysplit atmospheric transport and dispersion modeling system. Bull. Am. Meteorol. Soc. 96, 2059–2077. https://doi.org/10.1175/BAMS-D-14-00110.1.

Stunder, B.J.B., 1996. An assessment of the quality of forecast trajectories. J. Appl. Meteorol. 35, 1319–1331.

Taiwo, A.M., Beddows, D.C.S., Calzolai, G., Harrison, R.M., Lucarelli, F., Nava, S., Shi, Z., Valli, G., Vecchi, R., 2014. Receptor modelling of airborne particulate matter in the vicinity of a major steelworks site. Sci. Total Environ. 490, 488–500. https://doi.org/10.1016/j.scitotenv.2014.04.118.

Titos, G., Lyamani, H., Pandolfi, M., Alastuey, A., Alados-Arboledas, L., 2014. Identification of fine (PM1) and coarse (PM10-1) sources of particulate matter in an urban environment. Atmos. Environ. 89, 593–602. https://doi.org/10.1016/j.atmosenv.2014.03.001.

University of Oxford, Blavatnik School of Governement, 2020. Oxford COVID-19 Government Response Tracker (OxCGRT) [WWW Document]. URL. https://www.bsg.ox.ac.uk/%0Aresearch/research-projects/coronavirus-government-response-tracker (accessed 4.19.22).

US-EPA, 2014. EPA Positive M atrix Factorization (PM F) 5.0 Fundamentals and User guide, Environmental Protection Agency Office of Researc and Development, Publushing House Whashington, DC 20460.

Viana, M., Kuhlbusch, T.A.J., Querol, X., Alastuey, A., Harrison, R.M., Hopke, P.K., Winiwarter, W., Vallius, M., Szidat, S., Prévôt, A.S.H., Hueglin, C., Bloemen, H., Wåhlin, P., Vecchi, R., Miranda, A.I., Kasper-Giebl, A., Maenhaut, W., Hitzenberger, R., 2008. Source apportionment of particulate matter in Europe: a review of methods and results. J. Aerosol Sci. 39, 827–849. https://doi.org/10.1016/j.jaerosci.2008.05.007.

Viana, M., Amato, F., Alastuey, A., Querol, X., Moreno, T., Dos Santos, S.G., Herce, M.D., Fernández-Patier, R., 2009. Chemical tracers of particulate emissions from commercial shipping. Environ. Sci. Technol. 43, 7472–7477. https://doi.org/10.1021/es901558t.

Vicente, E.D., Vicente, A., Evtyugina, M., Carvalho, R., Tarelho, L.A.C., Oduber, F.I., Alves, C., 2018. Particulate and gaseous emissions from charcoal combustion in barbecue grills. Fuel Process. Technol. 176, 296–306. https://doi.org/10.1016/j.fuproc.2018.03.004.

Wang, H., Miao, Q., Shen, L., Yang, Q., Wu, Y., Wei, H., 2021b. Air pollutant variations in Suzhou during the 2019 novel coronavirus (COVID-19) lockdown of 2020: high time-resolution measurements of aerosol chemical compositions and source apportionment. Environ. Pollut. 271, 116298 https://doi.org/10.1016/j.envpol.2020.116298.

Wang, Y., Liu, B., Zhang, Y., Dai, Q., Song, C., Duan, L., Guo, L., Zhao, J., Xue, Z., Bi, X., Feng, Y., 2021a. Potential health risks of inhaled toxic elements and risk sources during different COVID-19 lockdown stages in Linfen, China. Environ. Pollut. 284, 117454 https://doi.org/10.1016/j.envpol.2021.117454.

WHO, 2021. WHO Global Air Quality Guidelines 1–360..

World Health Organization, 2013. Health effects of particulate matter: policy implications for counstries in Eastern Europe, Caucasus and central Asia. J. Korean Med. Assoc. https://doi.org/10.5124/jkma.2018.61.12.749.

Zanobetti, A., Franklin, M., Koutrakis, P., Schwartz, J., 2009. Fine particulate air pollution and its components in association with cause-specific emergency admissions. Environ. Heal. A Glob. Access Sci. Source 8, 1–12. https://doi.org/10.1186/1476-069X-8-58/FIGURES/2.

Zheng, H., Kong, S., Chen, N., Yan, Y., Liu, D., Zhu, B., Xu, K., Cao, W., Ding, Q., Lan, B., Zhang, Z., Zheng, M., Fan, Z., Cheng, Y., Zheng, S., Yao, L., Bai, Y., Zhao, T., Qi, S., 2020. Significant changes in the chemical compositions and sources of PM2.5 in Wuhan since the city lockdown as COVID-19. Sci. Total Environ. 739 https://doi.org/10.1016/j.scitotenv.2020.140000.